

# Lawrence Berkeley National Laboratory

## LBL Publications

### Title

THE EFFECT OF MICROSTRUCTURE ON FATIGUE CRACK GROWTH IN DUPLEX FERRITE-MARTENSITE STEELS

### Permalink

<https://escholarship.org/uc/item/0td095mr>

### Author

Lawrence Berkeley National Laboratory

### Publication Date

1982-06-01



# Lawrence Berkeley Laboratory

UNIVERSITY OF CALIFORNIA

## Materials & Molecular Research Division

RECEIVED  
LAWRENCE  
BERKELEY LABORATORY

JUN 7 1982

LIBRARY AND  
DOCUMENTS SECTION

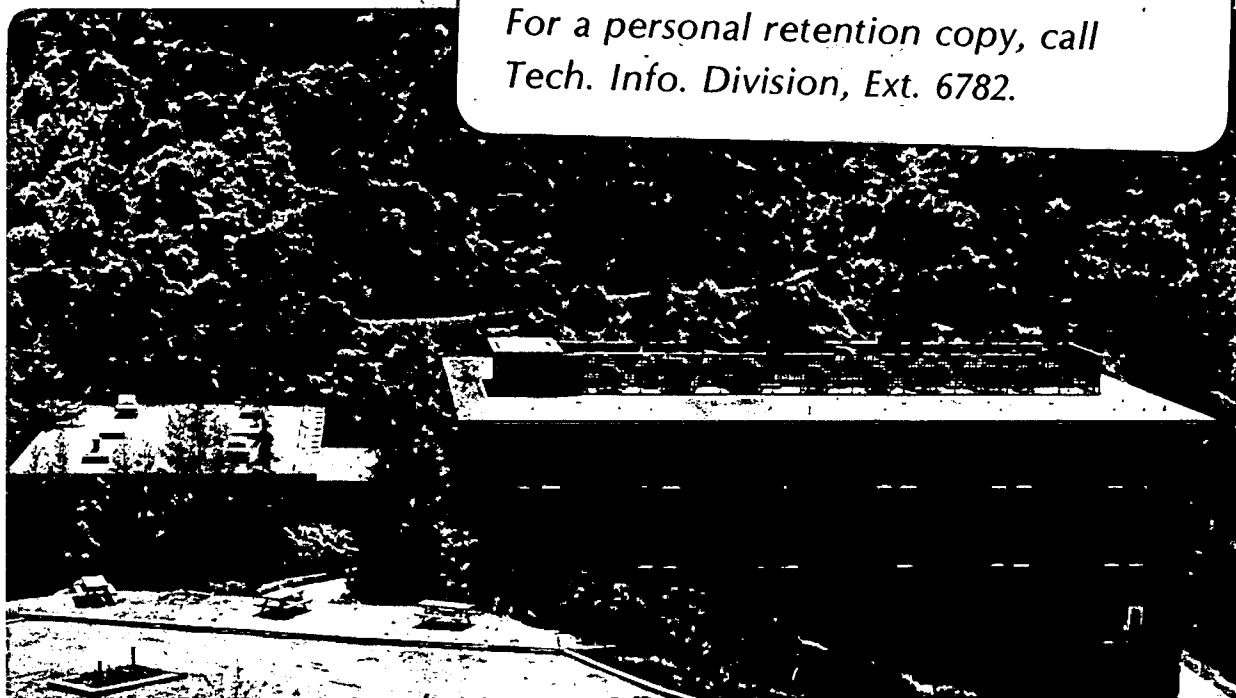
THE EFFECT OF MICROSTRUCTURE ON FATIGUE CRACK GROWTH  
IN DUPLEX FERRITE-MARTENSITE STEELS

James A. Wasynczuk  
(M.S. thesis)

June 1982

### TWO-WEEK LOAN COPY

*This is a Library Circulating Copy  
which may be borrowed for two weeks.  
For a personal retention copy, call  
Tech. Info. Division, Ext. 6782.*



LBL-15110

## DISCLAIMER

This document was prepared as an account of work sponsored by the United States Government. While this document is believed to contain correct information, neither the United States Government nor any agency thereof, nor the Regents of the University of California, nor any of their employees, makes any warranty, express or implied, or assumes any legal responsibility for the accuracy, completeness, or usefulness of any information, apparatus, product, or process disclosed, or represents that its use would not infringe privately owned rights. Reference herein to any specific commercial product, process, or service by its trade name, trademark, manufacturer, or otherwise, does not necessarily constitute or imply its endorsement, recommendation, or favoring by the United States Government or any agency thereof, or the Regents of the University of California. The views and opinions of authors expressed herein do not necessarily state or reflect those of the United States Government or any agency thereof or the Regents of the University of California.

THE EFFECT OF MICROSTRUCTURE ON FATIGUE CRACK GROWTH  
IN DUPLEX FERRITE-MARTENSITE STEELS

James A. Wasynczuk

Materials and Molecular Research Division  
Lawrence Berkeley Laboratory  
and Department of Materials Science and Mineral Engineering  
University of California, Berkeley, California 94720

ABSTRACT

Monotonic tensile and fatigue crack growth tests have been performed on AISI 1018 and Fe/2Si/0.1C steels with duplex ferrite-martensite (DFM) microstructures. The effect of microstructure on mechanical properties was examined.

Two distinct martensite distributions were produced in AISI 1018 DFM. The primary differences between the two were ferrite and martensite particle sizes. It was found that tensile fracture was sensitive to both martensite distribution and volume fraction. For a given volume fraction of martensite, large particle sizes increased strength but drastically reduced ductility. The volume fraction of martensite influenced tensile properties according to the "rule of mixtures."

Threshold stress intensity ranges for fatigue crack growth in AISI 1018 DFM were found to be unaffected by the distribution nor the volume fraction of martensite. Mid-growth range fatigue crack growth rates in AISI 1018 DFM were increased when particle sizes were large. The increased crack growth rates were attributed to crack extension by cleavage fracture in ferrite. The Fe/2Si/0.1C DFM alloy was found to have a considerably higher fatigue threshold stress intensity than

AISI 1018 DFM of comparable strength. The greater fatigue threshold stress intensity in Fe/2Si/0.1C DFM was attributed to crack closure effects.

THE EFFECT OF MICROSTRUCTURE ON FATIGUE CRACK GROWTH  
IN DUPLEX FERRITE-MARTENSITE STEELS

Table of Contents

	Page
ABSTRACT . . . . .	i
I. INTRODUCTION . . . . .	1
II. EXPERIMENTAL PROCEDURE . . . . .	5
A. Materials Preparation . . . . .	5
B. Heat Treatment . . . . .	5
C. Mechanical Testing . . . . .	6
1. Tensile Testing . . . . .	6
2. Fatigue Crack Growth . . . . .	7
D. Metallography . . . . .	9
1. Optical Metallography . . . . .	9
2. Scanning Electron Microscopy . . . . .	9
3. Transmission Electron Microscopy . . . . .	11
III. RESULTS . . . . .	12
A. Microstructure . . . . .	12
1. Optical and Scanning Electron Microscopy . . . . .	12
2. Transmission Electron Microscopy . . . . .	15
B. Mechanical Properties . . . . .	16
1. Monotonic Tensile Properties . . . . .	16
2. Fatigue Crack Growth . . . . .	17
C. Fractography . . . . .	18
1. Monotonic Tensile Fracture . . . . .	18

	Page
2. Fatigue Fracture . . . . .	19
IV. DISCUSSION . . . . .	25
A. Tensile Data . . . . .	25
B. Fatigue Data . . . . .	27
V. CONCLUSIONS . . . . .	34
ACKNOWLEDGEMENTS . . . . .	35
REFERENCES . . . . .	36
TABLES . . . . .	41
FIGURE CAPTIONS . . . . .	44
FIGURES . . . . .	47

## I. INTRODUCTION

Duplex ferrite-martensite (DFM), or dual phase, steels have microstructures which consist mainly of hard 'martensite' particles embedded in a soft ferrite matrix. These microstructures are produced by a variety of thermal and thermomechanical treatments, all of which involve cooling a composite of ferrite + austenite at a rate sufficient to transform austenite to 'martensite'.\* Monotonic tensile properties characteristic to DFM steels are low yield strength to tensile strength ratios, continuous yielding behavior, high initial strain hardening rates, and good ductility. These properties make DFM steels attractive materials for applications where both formability and strength are required.

Although experiments aimed at obtaining desirable mechanical properties from DFM microstructures were reported as early as 1967,<sup>1</sup> research and development of DFM steels did not become extensive until around 1975.<sup>2,3</sup> The impetus for most of the research has been the automobile industry's need to produce more fuel efficient vehicles via weight reduction. By using DFM steels the strength to weight ratio of many formed components can be improved over what was obtained previously with high-strength low-alloy (HSLA) steels that have conventional microstructures of ferrite + pearlite. While the automobile industry is the major user of DFM steels, it has recently been shown that DFM steels may also be successfully used in low temperature structural applications.<sup>4</sup>

---

\*'Martensite' is in quotation because ferrite-bainite composites also exhibit dual-phase characteristics.<sup>4</sup>



Since the study of DFM steels was started at Berkeley by Thomas and Koo,<sup>5</sup> the effects of different metallurgical variables such as martensite volume fraction,<sup>6</sup> morphology,<sup>7</sup> carbon content,<sup>6</sup> and alloy additions<sup>8-11</sup> have been examined. With the detailed observations of microstructural features and the measurements of mechanical properties acquired from these investigations, microstructure-property relationships have been developed. The mechanical tests performed in these investigations were monotonic tension, Charpy impact, and Vickers microhardness. Since fatigue is an important aspect of engineering design as well as of fundamental materials behavior, this study was initiated in order to further develop microstructure-property relationships for superior performance DFM steels.

Research on fatigue of DFM steels has been concentrated in three areas: (1) cyclic stress-strain and strain-life behaviors, (2) direct observation of nonpropagating microcracks at the endurance limit, and (3) threshold behavior and fatigue crack growth of long cracks.

#### (1) Cyclic Stress-Strain and Strain-Life Behavior

The cyclic stress-strain and strain-life behavior of a vanadium containing HSLA steel\* with both 'as received' (ferrite + pearlite) and DFM (16.5 volume percent martensite) microstructures were examined by Davies.<sup>12</sup> The 'as received' steel exhibited cyclic softening at cyclic strain ( $\epsilon$ ) amplitudes less than  $\frac{\Delta\epsilon}{2} = 0.003$  and cyclic hardening at higher cyclic strain amplitudes. The DFM steel showed rapid cyclic hardening at all cyclic strain amplitudes. Cyclic strain-life behavior was similar for both steels. The 'as received' steel, which possessed the higher

---

\* Jones and Laughlin, Van-80.

yield strength, showed longer fatigue life at small cyclic strain amplitudes ( $\frac{\Delta\epsilon}{2} < 0.003$ ), whereas the DFM steel lasted longer at high cyclic strain amplitudes.

The effect of martensite volume fraction on the cyclic stress-strain and strain-life behaviors of this DFM steel has also been examined.<sup>13</sup> When martensite volume fractions were less than 31% this DFM steel exhibited cyclic hardening. At higher martensite volume fractions cyclic softening was observed. Although monotonic yield strength increased with martensite volume fraction according to the 'law of mixtures,'<sup>6</sup> no such relationship was found for cyclic yield strength. Cyclic yield strength increased with martensite volume fraction in the range of 16.5% to 31% martensite only. Further increases in martensite volume fraction, up to 60%, did not change cyclic yield strength. Similarly, the fatigue life of this DFM steel increased with martensite volume fraction in the range of 16.5% to 31% only. Further increases in martensite volume fraction reduced fatigue life.

(2) Direct observation of nonpropagating microcracks at the endurance limit.

Kunio et al.<sup>14,15</sup> have directly observed short, 200-500  $\mu\text{m}$ , nonpropagating fatigue cracks in DFM steels that were fatigued at the endurance limit. It was found that all nonpropagating cracks in the ferrite matrix were stopped by martensite particles. The endurance limit was therefore interpreted as the critical alternating stress required for crack propagation through martensite. Moreover, it was found that the condition required for crack propagation through martensite was a critical combination of alternating stress and crack length. Under the

assumption that linear elastic fracture mechanics is applicable to these experiments, the critical combination of alternating stress and crack length was evaluated as the threshold alternating stress intensity for crack propagation through the martensite.

While the experimental results of Kunio et al. are meaningful in assessing the physical interpretation of the endurance limit in DFM steels, it should be recognized that, because the size of the short cracks were of the same order as microstructural features, their application of linear elastic fracture mechanics is somewhat suspect, and that the threshold stress intensity so determined is not the same as that determined for long cracks.

(3) Fatigue crack growth and threshold behavior of long cracks.

It has been proven that fracture mechanics concepts can be applied to fatigue crack growth of long cracks.<sup>16</sup> A material's resistance to fatigue crack growth is generally evaluated by the relationship between alternating stress intensity and crack growth rate.<sup>16,17</sup> The fatigue threshold is the value of alternating stress intensity at which the crack growth rate is so low that it can be considered negligible for most situations.

Fatigue crack growth and threshold behavior of long cracks in DFM steels have been investigated by Suzuki and McEvily<sup>18</sup> and Minakawa and McEvily.<sup>19</sup> Because the nature of these investigations is similar to that of this thesis, their results are included in the Discussion section.

## II. EXPERIMENTAL PROCEDURE

### A. Materials Preparation

One of the materials used in this investigation was AISI 1018 steel, nominal composition, according to ASTM specification A29, 0.15 to 0.20 wt. pct. C/0.60 to 0.90% Mn/0.040% max. P/0.050% max. S. This steel was purchased in the form of 6.4 mm x 63.5 mm ( $\frac{1}{4}$  in x  $2\frac{1}{2}$  in) cold rolled bar.

The other steel studied was the experimental alloy of nominal composition Fe/2.0% Si/0.2% C.<sup>1</sup> The alloy was supplied by Sandia National Laboratory, Albuquerque, N.M. It was cast in a 23 kg. (50 lb.) ingot and fully killed with rare earth elements, vacuum arc remelted, and homogenized for 24 hours. The ingot was then forged at 1000°C to 76.2 mm (3 in.) square bars, controlled rolled to 19 mm ( $\frac{3}{4}$  in.) plate, and then cold rolled to 12.7 mm ( $\frac{1}{2}$  in.) plate - the condition in which it was sent to Berkeley. The 12.7 mm plate was then hot rolled at 1000°C to 8 mm ( $\frac{5}{16}$  in.) plate.

Oversized flat tensile and compact blanks were cut from the flat plates with the tensile axis parallel to the rolling direction. The dimensions of the blanks were approximately 6.4 mm x 15.9 mm x 69.8 mm ( $\frac{1}{4}$  in. x  $\frac{5}{8}$  in. x  $2\text{-}\frac{3}{4}$  in.) and 6.4 mm x 60.3 mm x 63.5 mm ( $\frac{1}{4}$  in. x  $2\text{-}\frac{3}{8}$  in. x  $2\frac{1}{2}$  in.), respectively.

### B. Heat Treatment

DFM microstructures were obtained by two methods: (1) Intercritical anneal; (a) anneal at a two phase,  $\alpha+\gamma$ , temperature for  $\frac{1}{2}$  hour, (b) quench in ice water. (2) Intermediate quench; (a) austenitize for

1 hour; (b) quench in ice water; (c) anneal at a two phase,  $\alpha+\gamma$ , temperature for  $\frac{1}{2}$  hour; and (d) quench in ice water.

In order to examine the effect of  $\alpha+\gamma$  annealing time on DFM microstructure and tensile properties,  $\alpha+\gamma$  annealing time was increased to 4 hours for two sets of specimens.

Austenitizing and  $\alpha+\gamma$  annealing temperatures are listed in Table I. Austenitization and  $\alpha+\gamma$  annealing above 800°C were done in a vertical tube furnace under a flowing argon atmosphere. All other  $\alpha+\gamma$  annealing treatments were done in a horizontal box furnace with an unprotected atmosphere. Three tensile blanks were heat treated simultaneously. Compact blanks were heat treated singly.

### C. Mechanical Testing

#### 1. Tensile Testing

Tensile specimens were 6.4 mm ( $\frac{1}{4}$  in.) thick flat bars with a 25.4 mm (1 in.) gage length. After heat treatment, the oversized blanks were ground under flood cooling to ASTM specification E8-69, Fig. (1a). Approximately 0.4 mm (0.015 in.) was ground from each surface to remove any decarburized material (decarburization was observed to be less than 0.4 mm).

Tensile tests were performed at room temperature on both an Instron screw drive machine and a MTS electro-servo-hydraulic machine with a cross-head speed of 0.5 mm/sec. The effect of the testing machine on tensile properties was negligible. Total elongations were determined by measuring 25.4 mm (1 in.) marks on the gage before and after testing. The other tensile properties were determined from the recorded load-cross-head displacement curves. Yield strengths were determined by the 0.2% offset method.

## 2. Fatigue Crack Growth

Fatigue crack growth tests were performed with 6.4 mm ( $\frac{1}{4}$ " ) thick compact tension specimens, Fig. (1b). The surface grinding procedure used on these specimens was the same as used for the tensile specimens. Specimens were cycled, under load control, on a MTS 20 kip electro-servo-hydraulic testing machine. The applied load was sinusoidal tension at a load ratio ( $R = K_{\min}/K_{\max}$ ) of 0.05 where  $K_{\min}$  and  $K_{\max}$  are the minimum and maximum stress intensities during each cycle. The stress intensity factor was calculated with the following expression:

$$K = \frac{P}{BW^{3/2}} \left[ 29.6 \left(\frac{a}{w}\right)^{1/2} - 185.5 \left(\frac{a}{w}\right)^{3/2} + 655.7 \left(\frac{a}{w}\right)^{5/2} - 1017 \left(\frac{a}{w}\right)^{7/2} + 638.9 \left(\frac{a}{w}\right)^{9/2} \right],$$

where  $a$  is the crack length and  $w$  the specimen width. The cyclic frequency was 50 Hz. The test environment was laboratory air maintained at a constant temperature of 21°C and a constant relative humidity of 50 percent. Crack length was monitored continuously using the electric potential method.<sup>20,21</sup> It was experimentally verified that the apparatus used could measure absolute crack length to within 0.1 mm.

Thresholds were determined by a load shedding procedure in which  $\Delta K$  ( $\Delta K = K_{\max} - K_{\min}$ ) was systematically reduced by increments of 10 percent or less. Crack growth rates ( $da/dN$ ) below  $10^{-6}$  mm/cycle were measured during the approach of threshold ( $\Delta K_0$ ). After each load reduction the crack was allowed to grow, at constant  $\Delta K$ , for a distance of at least three times the monotonic plane strain plastic zone

size\* that corresponded to a crack growth rate of  $10^{-6}$  mm/cycle. Little difference in  $da/dN$  was found if measurements were made after the crack grew, at constant  $\Delta K$ , through the previous monotonic plastic zone.

$\Delta K_0$  was defined as the alternating stress intensity at which less than 0.1 mm of crack growth occurred in  $3 \times 10^6$  cycles. This corresponds to a crack growth rate of  $3.3 \times 10^{-8}$  mm/cycle or less. At least three specimens were fatigue tested for each heat treatment. The load shedding procedure used was such that  $\Delta K_0$  was usually achieved at a crack length of  $20.5 \text{ mm} < a < 21.5 \text{ mm}$ .

On some specimens  $\Delta K_0$  was determined the first time at  $a \approx 21 \text{ mm}$ ,  $\Delta K$  was increased and the load shedding procedure was repeated so that  $\Delta K_0$  was again achieved at  $a \approx 25 \text{ mm}$ . No significant difference was found between the two thresholds.

After  $\Delta K_0$  was determined, load was increased such that  $da/dN \approx 10^{-6}$  mm/cycle and then maintained constant until termination of the test. Values of  $da/dN$  below  $10^{-6}$  mm/cycle were obtained during the load shedding procedure. Crack growth rates above  $10^{-6}$  mm/cycle were determined by numerical differentiation of curves of crack length versus number of cycles.

---

\* The monotonic plane strain plastic zone size was approximated by

$$\frac{1}{6\pi} \left( \frac{K_{\max}}{S_y} \right)^2$$

where  $S_y$  is the monotonic yield stress.<sup>22,23</sup>

## D. Metallography

### 1. Optical Metallography

Sections for optical metallography were taken either from the gage length of broken tensile specimens or from compact specimens close to the crack path. For a given heat treatment, the microstructural features were the same for both of the section types.

After mounting the sections in either bakelite or kold-mount, they were rough ground on a flood cooled 180 grit belt and then hand ground on wet silicon carbide paper from 240 grit to 600 grit. Polishing was done with 6  $\mu\text{m}$  diamond paste on a nylon covered polishing wheel followed by either 1  $\mu\text{m}$  diamond paste on nylon or a 0.3  $\mu\text{m}$  alumina slurry on felt. Microstructural features of the DFM structures were revealed by etching in either a 5% or a 2% nital solution. Prior austenite grain sizes were revealed by tempering at 500°C for 4 hours and etching with picral. Grain size was determined by a line intercept technique.<sup>24</sup> Metallographic observation was done with a Zeiss ultraphot II metallograph. Martensite volume fractions were determined by a point fraction method.<sup>24</sup>

### 2. Scanning Electron Microscopy

#### 2.1. Metallography

Martensite and ferrite particle sizes were measured from scanning electron micrographs of specimens prepared for optical metallography. Magnification greater than what could readily be achieved by optical microscopy was required to resolve the dimensions of the smaller particles. Particle size is defined as the average line length contained within a particle. It was determined by edge to edge measurement of



individual particles along a test line.\* The connectivity of martensite is defined by the parameter  $\psi$ , where  $\psi = N_{\alpha/\gamma}/N_{\alpha/\gamma} + N_{\alpha/\alpha}$ .  $N_{\alpha/\gamma}$  is the average number of intersections with ferrite/martensite phase boundaries per unit length ( $\text{mm}^{-1}$ ) and  $N_{\alpha/\alpha}$  is the average number of intersections with ferrite/ferrite grain boundaries per unit length ( $\text{mm}^{-1}$ ). 18,25

## 2.2. Fractography

Tensile and fatigue fracture surfaces were examined using an AMR-1000 scanning electron microscope operated at 20 kV. Taper sections of fracture surfaces were cut at  $\sim 5^\circ$ . Percent of cleavage fracture was determined by a point fraction technique.<sup>24</sup> Each data point in the plot of  $\Delta K$  versus percent cleavage fracture is a result of point fraction measurement on one 200X mid-thickness fractograph only, so the line fitting the data may not be representative of the situation across the entire crack front.

Near-threshold fatigue crack path was determined by examining specimens containing cracks that were stopped at near threshold crack growth rates ( $da/dN < 10^{-7}$  mm/cycle). For these specimens  $\Delta K$  was systematically reduced by the usual load shedding procedure. Cracks were grown just above threshold for a minimum of 0.2 mm and then stopped. The specimens were then sectioned, and the crack profile was examined, both optically and with SEM, at approximately mid-thickness.

---

\* A 100 mm test line length on 1000X micrographs was used. Optical micrographs at 400X were used to measure 'as received' ferrite and pearlite particle sizes.

### 3. Transmission Electron Microscopy

Thin foils for transmission electron microscopy were obtained from compact specimens near the crack path. Slices of approximately 25 mils were slow cut with a 1/32 in. silicon carbide abrasive disc under flood cooling. The slices were chemically thinned to 2-3 mils at room temperature in a solution of 96 ml of 30%  $H_2O_2$  and 4 ml of 48% HF. After the 3 mm discs were spark cut from these slices they were hand ground on 600 grit silicon carbide paper to remove any oxide layer. The discs were polished to thin foils at room temperature in a twin jet electropolisher using a chromic-acetic acid solution. Polishing potentials from 35-50 volts were used. The thin foils were stored in 200 proof ethyl alcohol and later examined in either a Hitachi HU 125 or Phillips EM 301 transmission electron microscope at an accelerating voltage of 100 kV.

### III. RESULTS

#### A. Microstructure

##### 1. Optical and Scanning Electron Microscopy

###### (i) AISI 1018

Optical micrographs of the as received martensitic, and DFM structures are shown in Fig. (2). Higher magnification SEM micrographs of the DFM structures are shown in Fig. (3). Mean values of quantitative metallographic measurements are listed in Table II.

The principal differences between the two types of DFM structures were martensite distribution and ferrite grain size. Martensite distribution depends on the structure that existed just prior to  $\alpha+\gamma$  annealing.

In the intercritical anneal heat treatment the structure prior to  $\alpha+\gamma$  annealing was cold worked ferrite and pearlite. The primary sites for austenite nucleation during  $\alpha+\gamma$  annealing were grain boundaries and ferrite-cementite interfaces. During  $\alpha+\gamma$  annealing, the transformation to austenite occurred mainly within pearlite grains and along  $\alpha/\alpha$  grain boundaries. Because the  $\alpha+\gamma$  annealing temperatures used were so high that the volume fraction of austenite approached 50%, almost all of the grain boundaries were decorated with austenite. Very few  $\alpha/\alpha$  grain boundaries existed in the DFM structure, so martensite connectivity was very high (>85%).

In the intermediate quench heat treatment the structure prior to  $\alpha+\gamma$  annealing was lath martensite. This structure consists of prior austenite grains that have transformed into arrays of parallel laths. These arrays are commonly called packets. Within a packet the

boundaries between adjacent laths are generally low angle type and are frequently associated with thin films of retained austenite.<sup>5,27</sup> The packets themselves are separated by high angle boundaries,<sup>26</sup> several packets occurring in one prior austenite grain. Prior austenite grain, packet, and lath boundaries are numerous and well dispersed in the lath martensite structure. All of these defects promote austenite nucleation during  $\alpha+\gamma$  annealing.

The preferential nucleation of austenite along prior austenite grain boundaries results in the formation of rings of interconnected martensite particles upon quenching. The average diameter of these rings is comparable to the prior austenite grain size,  $\sim 80 \mu\text{m}$  (see optical micrograph Fig. (2d)). Within the rings are many other martensite particles. The narrow shape of many of them suggests that they were formed from austenite that was nucleated at lath boundaries. These narrow particles break the ferrite matrix into a finer scale than that in structures produced by the intercritical anneal, DFM(IA), heat treatment (see SEM micrographs, Fig. (3)). As with the DFM(IA) structure, very few  $\alpha/\alpha$  grain boundaries can be resolved so martensite connectivity is high (>95%).

The quantitative metallographic results indicate that the microstructural quantity most strongly affected by the distribution of martensite was the mean ferrite particle size, which is equivalent to the mean ferrite line length  $\overline{L}_{\alpha}$ . Although the definition of  $\overline{L}_{\alpha}$  is the same for both DFM structures, the physical interpretation is different. For DFM(IA) structures  $\overline{L}_{\alpha}$  is a good measure of the ferrite grain size. For DFM(IQ) structures, however, the ferrite grain size is not so well defined. Because the ferrite in DFM(IQ) was formed by a tempering

process, it was crystallographically related to the martensite that existed prior to  $\alpha+\gamma$  annealing. Therefore, it was also related to the austenite from which the martensite transformed. Hence, the crystallographic orientation of the ferrite matrix was similar over a much larger range than  $\overline{L}_\alpha$  indicates, i.e., the packet size or the prior austenite grain size.

The range of martensite volume fractions obtainable in AISI 1018 is limited by the extent of the  $\alpha+\gamma$  phase field. 35% was the minimum volume fraction of martensite obtainable with the heat treatment technique used. Attempts at obtaining lower volume fractions of martensite resulted in microstructures of ferrite and spheroidized cementite. Even in the DFM structures with ~35% martensite some spheroidal carbides were observed.

Increasing the  $\alpha+\gamma$  annealing time from  $\frac{1}{2}$  hour to 4 hours caused no change in martensite distribution for the DFM(IA) structure. Annealing for 4 hours caused only minor changes in martensite distribution for the DFM(IQ) structure. Intergranular martensite particles became slightly larger and fewer in number. Martensite volume fraction was unchanged by longer annealing times.

(ii) Fe/2Si/0.1C

An optical micrograph of the Fe/2Si/0.1C DFM(IQ) structure is shown in Fig. (4). The crack in the structure is explained in the Fractography section. A high magnification SEM micrograph of Fe/2Si/0.1C DFM(IQ) is shown in Fig. (5). Mean values of quantitative metallographic measurements are listed in Table II.

One of the effects of the 2 wt.% Si in this alloy is to markedly reduce the tendency for the nucleation of  $\gamma$  on prior austenite grain boundaries during  $\alpha+\gamma$  annealing.<sup>1</sup> Si also extends the  $\alpha+\gamma$  two phase field.<sup>2</sup> It should also be noted that the ferrite particle size in Fe/2Si/0.1C DFM(IQ) is larger than that in AISI 1018 DFM(IQ). The microstructure of this steel has been well characterized in previous reports.<sup>1,2,7</sup>

## 2. Transmission Electron Microscopy

Through transmission electron microscopy it was verified that the hard phase of the composite was indeed martensite and not some other lower transformation product. Figs. (6a) and (6b) are transmission electron micrographs of AISI 1018 DFM(IQ) with 46 vol.% martensite. Fig. (6a) shows two martensite particles surrounded by heavily dislocated ferrite. Substructural twins are evident in the martensite particles. Fig. (6b) shows martensite particles and subgrains within the ferrite matrix. The fine structure of these and other DFM microstructures have been thoroughly characterized in previous reports.<sup>1,2,5,7-11,27</sup>

## B. Mechanical Properties

### 1. Monotonic Tensile Properties

#### (i) AISI 1018

At equivalent volume fractions of martensite, AISI 1018 DFM(IA) displayed higher yield and ultimate tensile strengths, but considerably less uniform and total elongations than AISI 1018 DFM(IQ). For example, at ~36% vol.% martensite, AISI 1018 DFM(IA) gave ~15% higher yield strength, ~7% greater U.T.S., but only about half of the uniform and total elongations of AISI 1018 DFM(IQ). These differences are illustrated in the stress-strain curves shown in Fig. (7). The tensile properties of DFM and martensitic structures are listed in Table III and plotted versus martensite volume fraction in Fig. (8).

"Mixture rule" behavior, a linear increase in the strength of the composite with increased volume fraction of martensite,<sup>6</sup> was exhibited by both DFM structures. Tensile elongation of the DFM(IA) structure, however, was not strongly affected by the martensite volume fraction.

Tensile properties of the DFM structures that were  $\alpha+\gamma$  annealed for 4 hours were, within experimental error, equivalent to those of the DFM structures that were  $\alpha+\gamma$  annealed for  $\frac{1}{2}$  hour. Data are listed in Table III.

#### (ii) Fe/2Si/0.1C

Tensile data for Fe/2Si/0.1C DFM(IQ) are included in Table III and Fig. (7). Tensile properties of Fe/2Si/0.1C DFM(IQ) were similar to those of AISI 1018 DFM(IQ) at comparable martensite volume fraction.

## 2. Fatigue Crack Growth

### 2.1. Threshold Alternating Stress Intensity

#### (i) AISI 1018

Within experimental error, the mean values of threshold alternating stress intensity,  $\Delta K_o$ , were the same for all AISI 1018 DFM structures tested. Measured values of  $\Delta K_o$  ranged from 8.0 MPa $\sqrt{m}$  to 10.9 MPa $\sqrt{m}$ . Data are presented in Table IV.

#### (ii) Fe/2Si/0.1C

The mean value of  $\Delta K_o$  for Fe/2Si/0.1C DFM(IQ) at 41 vol.% martensite was 15.8 MPa $\sqrt{m}$ . This is significantly greater than the mean value of 9.7 MPa $\sqrt{m}$  which was obtained for AISI 1018 DFM(IQ) at 35 vol.% martensite. Threshold data for Fe/2Si/0.1C are included in Table IV.

### 2.2. Mid-Growth Regime

#### (i) AISI 1018

The effect of martensite distribution on fatigue crack growth in AISI 1018 DFM was most pronounced for growth rates above  $10^{-5}$  mm/cycle. In this regime the slope of the log  $\Delta K$  versus log  $da/dN$  curve was steeper for DFM(IA) than DFM(IQ). Shown in Fig. (9) are crack growth curves for AISI 1018 DFM(IA) at 37 vol.% martensite and AISI 1018 DFM(IQ) at 35 vol.% martensite. The trend of higher crack growth rates for DFM(IA) was identical for the DFM structures with larger volume fractions of martensite. Crack growth curves for the DFM structures with ~47 vol.% martensite were nearly coincident with those in Fig. (9).

Data in the mid-growth range of fatigue crack growth followed an exponential relationship of the form  $\frac{da}{dN} = C \Delta K^m$ , where C is a constant and m is often called the Paris law exponent.<sup>16,17</sup> Paris law exponents



were approximated by measuring the slope of the best straight line drawn through data points in the range of  $10^{-5}$  mm/cycle to  $10^{-3}$  mm/cycle. Values are listed in Table IV.

(ii) Fe/2Si/0.1C

The mid-range fatigue crack growth curve of Fe/2Si/0.1C DFM(IQ) can be divided into two regions. For crack growth rates between  $10^{-5}$  mm/cycle and  $10^{-4}$  mm/cycle the slope of the crack growth curve was extremely steep, much steeper than any of the other curves presented. Above crack growth rates of  $10^{-4}$  mm/cycle ( $\Delta K \sim 33 \text{ MPa}\sqrt{\text{m}}$ ), the crack growth curve of Fe/2Si/0.1C DFM(IQ) paralleled that of AISI 1018 DFM(IQ).

### C. Fractography

#### 1. Monotonic Tensile Fracture

(i) AISI 1018

Scanning electron microscope (SEM) observations of tensile specimen fracture surfaces indicated that the fracture mode for both AISI 1018 DFM structures was a mixture of dimple rupture and transgranular cleavage. Transgranular cleavage was the primary mode of fracture in AISI 1018 DFM(IA), Fig. (10a), while in AISI 1018 DFM(IQ) dimple rupture predominated, Fig. (10b). Observation of taper sections revealed that transgranular cleavage took place in the ferrite matrix, Fig. (10c). Inclusions were observed on all fracture surfaces.

(ii) Fe/2Si/0.1C

Tensile fracture in Fe/2Si/0.1C DFM(IQ) was exclusively ductile rupture.

## 2. Fatigue Fracture

### 2.1. Threshold Range

#### (i) AISI 1018

Low magnification ( $\sim 5X$ ) optical fractographs of the fatigue fracture surfaces of AISI 1018 DFM(IA) and AISI 1018 DFM(IQ) are shown in Figs. (11a) and (11b), respectively. The notches along the slides of the specimens were placed there after testing so that the approximate crack length could be readily obtained during SEM observation. SEM fractographs of the near-threshold fatigue fracture surfaces of AISI 1018 DFM(IA) and AISI 1018 DFM(IQ) are shown in Figs. (12a) and (12b), respectively. At this level of magnification (50X), the near-threshold fatigue fracture surfaces of both AISI 1018 DFM steels have similar appearance.

Higher magnification SEM fractographs of the near-threshold fatigue fracture surface of AISI 1018 DFM(IQ) are shown in Figs. (13a) and (13b), which were taken from the same region. The outline in Fig. (13a) surrounds a fractographic feature whose dimensions are on the order of the prior austenite grain size for that steel ( $\sim 80 \mu\text{m}$ ). In Fig. (13b) it can be seen that this feature represents a slight depression in the average fracture profile of the surrounding area.

The paths of the near-threshold fatigue cracks were found to be insensitive to the distribution of martensite. Fig. (14a) is an optical micrograph of a near-threshold fatigue crack in AISI 1018 DFM(IA). Fig. (14b) is a higher magnification SEM micrograph of the same crack. It is apparent that the crack traverses both martensite particles and ferrite grains. Similar behavior was observed in AISI 1018 DFM(IQ).

The near-threshold fatigue crack path in AISI 1018 DFM(IQ) was

also found to be transgranular with respect to the prior austenite grains. Fig. (15a) is an optical micrograph of a near-threshold fatigue crack in AISI 1018 DFM(IQ). The specimen was tempered and etched to reveal the prior austenite grains. Note that there is a marked deviation in the path of the crack within a large prior austenite grain. It could not be ascertained from this micrograph whether the changes in the crack path that occurred within that prior austenite grain are associated with prior martensite packet boundaries.

(ii) Fe/2Si/0.1C

A low magnification optical fractograph of a fatigue fracture surface of Fe/2Si/0.1C DFM(IQ) is shown in Fig. (11c). Even at this level of magnification it is apparent that the fracture surface topography of Fe/2Si/0.1C DFM(IQ) has a coarser appearance than those of the AISI 1018 DFM steels. The greater coarseness of fracture surface topography is well illustrated in Fig. (12), where Fig. (12c) is a fractograph of near-threshold fatigue fracture in Fe/2Si/0.2C DFM(IQ). It should be noted that the low magnification optical fractograph of Fe/2Si/0.2C DFM(IQ), Fig. (11c), also reveals that the oxide layer that delineates the position of the crack front at threshold<sup>28</sup> is curved across the thickness of the specimen. The effects of crack front curvature are considered below.

Like AISI 1018 DFM(IQ), the near-threshold fatigue fracture surfaces of Fe/2Si/0.2C DFM(IQ) contained features with dimensions comparable to the prior austenite grain size. Figs. (13c) and (13d) are SEM fractographs taken from the same region of near-threshold fatigue fracture in Fe/2Si/0.2C DFM(IQ). Fig. (13d) is a higher magnification

fractograph centered on a feature with dimensions comparable to the prior austenite grain size ( $\sim 180 \mu\text{m}$ ). In Fig. (13d) parallel "steps" can be seen within that feature. The widths of the "steps" are comparable to the ferrite and martensite particle sizes for this steel,  $8 \mu\text{m}$  and  $3 \mu\text{m}$ , respectively.

Very large ( $\sim 50 \mu\text{m}$ ) and abrupt changes in the fracture surface profile can be seen around the feature in the center of Fig. (13d). Such large and abrupt changes in fracture surface profile were common in near-threshold fatigue fracture of Fe/2Si/0.1C DFM(IQ). The distances between these abrupt changes in fracture surface profile were usually comparable to the prior austenite grain size. These abrupt changes in fracture surface profile are responsible for the coarse fracture surface topography shown in Fig. (12c).

As in AISI 1018 DFM(IQ), the near-threshold fatigue crack path in Fe/2Si/0.1C DFM(IQ) traversed both ferrite and martensite. Fig. (4) is an optical micrograph of a near-threshold fatigue crack in Fe/2Si/0.1C DFM(IQ).

The near-threshold fatigue crack path in Fe/2Si/0.1C DFM(IQ) was also transgranular with respect to prior austenite grains. Fig. (15b) is an optical micrograph of a near-threshold fatigue crack in Fe/2Si/0.1C DFM(IQ). The specimen was tempered and etched to reveal the prior austenite grains. Abrupt deviations in the crack path are shown in this micrograph. Note that the magnitude of the change in crack profile is greater in this steel than in AISI 1018 DFM(IQ). The abrupt deviations in the crack path occurred at boundaries. Whether they are prior austenite grain boundaries, or packet boundaries of the martensite that existed prior to  $\alpha+\gamma$  annealing, cannot be ascertained

from this micrograph, but the size of the regions that the boundaries divide suggests they are prior austenite grain boundaries.

It was noted that the low magnification optical fractograph of fatigue in Fe/2Si/0.1C DFM(IQ) (Fig. (11c)) revealed that the oxide layer that delineates the position of the crack front at threshold<sup>28</sup> was curved across the thickness of the specimen. Some curvature of the oxide layer was observed in almost all of the fatigue specimens tested in this study. It is thought that near-threshold fatigue crack growth was retarded at the sides of the specimens because of residual stresses that were brought about by the severe quench that followed  $\alpha+\gamma$  annealing. The effects of residual stresses on near-threshold fatigue crack growth in aluminum alloys have been thoroughly studied.<sup>29</sup> Although crack front curvature may have been responsible for some of the scatter in the threshold fatigue data, it is believed that the threshold stress intensities measured in this study are still valid because the presence of residual stresses was consistent for nearly all of the tests performed. It can also be argued that the crack closure effects responsible for the high value of threshold stress intensity in Fe/2Si/0.1C DFM(IQ) were also manifested in the mid-growth range, where the effects of residual stresses on crack growth are much less pronounced. Therefore, the high value of threshold stress intensity found for Fe/2Si/0.1C DFM(IQ) is real, but, quantitatively, it may not be exact. Furthermore, it was found that, for the case of AISI 1018 DFM(IA), with 37 vol.% martensite, crack front curvature had only a minor effect on threshold stress intensity. For one of the AISI 1018 DFM(IA) specimens, 1.0 mm, rather than the standard 0.4 mm, was ground from both sides of the specimen blank. Evidently, the

extra 0.6 mm of material removed was enough to eliminate the effects of residual stress on crack growth, for the near-threshold oxide layer in that specimen was flat across the entire thickness. The value of threshold stress intensity measured for the specimen with a flat crack front ( $9.0 \text{ MPa}\sqrt{\text{m}}$ ) was very close to the values obtained for specimens with curved crack fronts and identical microstructures.

## 2.1. Mid-Growth Range

### (i) AISI 1018

In the low magnification optical fractograph of the fatigue fracture surface of AISI 1018 DFM(IA), Fig. (11c), a great number of highly reflective facets can be seen. SEM observations revealed that the highly reflective facets were a consequence of transgranular cleavage of ferrite. Cleavage was widespread in fatigue fracture of AISI 1018 DFM(IA). It was observed over the entire range of applied  $\Delta K$ . Although the magnification in Fig. (12a) is insufficient to resolve them, occasional cleavage facets were observed even at near-threshold crack growth rates. As  $\Delta K$  increased, the occurrence of transgranular cleavage rose dramatically, becoming the principal mode of fracture at  $\Delta K \sim 26 \text{ MPa}\sqrt{\text{m}}$ . The strong increase in the percentage of cleavage fracture with  $\Delta K$  is illustrated in Fig. (16). As mentioned in the experimental procedure section, the line fitting the data may not necessarily represent the situation across the entire crack front.

Unlike the intercritical anneal structure, AISI 1018 DFM(IQ) maintained a ductile mechanism of crack extension throughout the range of applied  $\Delta K$ . Some isolated cleavage facets were observed at high

$\Delta K$ , but these were very few. The differences in crack growth mechanisms for the two DFM structures are illustrated in Fig. (17). Fig. (17a) and (17b) are mid-growth range fatigue fracture surfaces ( $\Delta K \approx 28 \text{ MPa}\sqrt{\text{m}}$ ) of AISI 1018 DFM(IA) and AISI 1018 DFM(IQ), respectively. Fig. (17c) and (17d) are taper sections of the same.

(11) Fe/2Si/0.1C

In the mid-growth range of fatigue crack growth in Fe/2Si/0.1C DFM(IQ), the fracture mode was ductile for all values of applied  $\Delta K$ . Occasional cleavage facets were observed where the applied  $\Delta K$  was very high ( $\approx 30 \text{ MPa}\sqrt{\text{m}}$ ), but their occurrence was sparse. However, a definite change in the fracture surface topography was observed well into the mid-growth range of fatigue crack growth.

In the low magnification optical fractograph of a fatigue fracture surface of Fe/2Si/0.1C DFM(IQ), Fig. (11c), an arrow indicates the position at which the transition in fracture surface topography occurred. That position corresponds to an applied  $\Delta K$  of  $\sim 33 \text{ MPa}\sqrt{\text{m}}$  and a crack growth rate of  $\sim 10^{-4} \text{ mm/cycle}$ . Although it is perhaps difficult to resolve in Fig. (11c), there is a definite change in the coarseness of fracture surface topography at that position. Although the change in fracture surface topography did not occur at the same crack length across the entire specimen thickness, SEM observations revealed that in some areas the change was very distinct. Fig. (18) is a SEM fractograph of such a distinct change in fracture surface topography. On the low  $\Delta K$  side of the transition the fracture surface has an appearance similar to that of near-threshold fatigue crack growth, Fig. (12c). On the high  $\Delta K$  side of the transition the large scale perturbations in fracture surface profile are absent.

#### IV. DISCUSSION

##### A. Tensile Data

The trend in tensile data was that for equivalent volume fractions of martensite, AISI 1018 DFM(IA) gave higher strength, but less elongation, than AISI 1018 DFM(IQ). The increased strength and reduced elongation are associated with a change in fracture mode from primarily ductile rupture to primarily transgranular cleavage of ferrite. A rationale for this behavior is that when large particles of ferrite are surrounded by large particles of martensite, plastic deformation of ferrite by slip is much reduced. The larger martensite particles of DFM(IA) restrict deformation of ferrite much more than the thin martensite particles of DFM(IQ). And, the larger ferrite particles of DFM(IA) permit more, and longer, dislocation pile-ups with concomitant stress concentrations that ultimately make cleavage the favorable mechanism of fracture.

While nonmetallic inclusions are certain to influence fracture behavior, it is assumed that their effect is identical for both DFM structures, i.e., the austenization performed in the intermediate quench heat treatment is assumed to have negligible effect on inclusion morphology.

Other transformation paths have been used to alter martensite distribution in AISI 1018 DFM steels. By thermal cycling between the  $\alpha + \gamma$  and  $\alpha + \text{Fe}_3\text{C}$  two phase fields and then quenching from  $\alpha + \gamma$  to DFM, Suzuki and McEvily produced a highly continuous network of martensite particles that encapsulated ferrite grains.<sup>18</sup> They labelled this kind of DFM microstructure "type B." It was compared to a microstructure



that was produced by continuous cooling from  $\gamma$  to  $\alpha+\gamma$  followed by quenching to DFM. The resulting microstructure, labelled "type A," consisted of isolated particles of martensite encapsulated by ferrite. For equivalent volume fractions of martensite, DFM(B) exhibited higher yield and tensile strengths, but much less elongation, than DFM(A). Presumably these changes in tensile properties were also due to constraint of ferrite plasticity.

However, the role of martensite connectivity in restricting ferrite plasticity is vague. Both of the DFM structures tested in this study were, by definition of  $\psi$ , highly continuous, a consequence of very few  $\alpha/\alpha$  grain boundaries. Yet, tensile fracture was much different between the two. On the other hand, the considerably stronger and less ductile DFM(B) structure was reported to have much higher martensite connectivity than DFM(A), 95% versus 35%. Therefore, it seems that martensite connectivity by itself is not an adequate parameter to describe mechanical behavior of the DFM composite. The size of the interconnected martensite particles must also be considered.

Analogous behavior of large particle sizes reducing ferrite plasticity has been reported for 0.1 carbon DFM steels.<sup>7,27</sup> However, for these lower carbon DFM steels much larger particle sizes were required in order for major changes in fracture mode to occur. In a previous study on the effect of martensite morphology on tensile deformation of Fe/2Si/0.1C DFM steel, Kim examined three types of DFM microstructures.<sup>7</sup> Two of the microstructures were produced by the (IA) and (IQ) heat treatments already described. The third DFM structure was produced by transforming high temperature austenite directly to  $\alpha+\gamma$  and then quenching to ferrite + martensite. This heat treatment,

called step quenching (SQ), produced a microstructure of very large ( $\sim 50 \mu\text{m}$ ) ferrite grains surrounding large ( $\sim 40 \mu\text{m}$ ) martensite grains. For approximately 40 vol.% martensite, tensile properties of Fe/2Si/0.1C DFM(IA) and DFM(IQ) were quite similar, with ductile rupture being the fracture mode for both structures. The strength was higher, and elongation much less, for the DFM(SQ) structure which failed primarily by transgranular cleavage of ferrite. It may be that the transition from ductile to cleavage fracture occurs at a larger particle size for 0.1 carbon DFM steels because martensite carbon concentration, and therefore martensite strength, is less than that of 0.18 carbon DFM steels with equivalent martensite volume fractions. Hence, larger particles of the weaker martensite are necessary to impose equivalent constraints on ferrite plasticity.

One complication in this analogy is that the 0.1 carbon DFM steels referred to were vacuum melted, and therefore the number of nonmetallic inclusions they contained was much less than in commercial AISI 1018. Although nonmetallic inclusions are certain to influence fracture behavior, the magnitude of change due to nonmetallic inclusions is believed to be small because tensile data for vacuum melted AISI 1020 DFM(IQ)<sup>27</sup> and commercial AISI 1018 DFM(IQ) are similar.

#### B. Fatigue Data

The higher fatigue crack growth rates exhibited by the AISI 1018 DFM(IA) steels in the range of  $10^{-5}$  to  $10^{-3}$  mm/cycle were associated with extensive transgranular cleavage fracture in ferrite. The effect of crack extension by transgranular cleavage causing accelerated fatigue crack growth is well established.<sup>30,31</sup> Crack extension by

transgranular cleavage is a process dominated by the maximum applied stress intensity, i.e., maximum tensile loading. The extensive cleavage fracture exhibited by AISI 1018 DFM(IA) can be explained by the same "reduction of ferrite plasticity" argument used in the discussion of tensile fracture.

Although the monotonic tensile properties of AISI 1018 DFM were significantly altered by changes in the distribution and volume fraction of martensite, the threshold stress intensities for fatigue crack growth were not. The threshold stress intensities of AISI 1018 DFM were nearly the same for all of the martensite distributions and volume fractions tested. However, Fe/2Si/0.1C DFM(IQ), a steel with monotonic tensile properties that were very similar to those of AISI 1018 DFM(IQ), gave a considerably higher threshold stress intensity than the AISI 1018 DFM steels. The fractographic results followed a trend parallel to the threshold fatigue data in that the near-threshold fatigue fracture surfaces of both AISI 1018 DFM(IA) and AISI 1018 DFM(IQ) had similar topographies while those of Fe/2Si/0.1C DFM(IQ) were much coarser by comparison. This correspondence between macroscopically coarse fracture surface topography and increased threshold stress intensity is consistent with recent ideas on fatigue crack closure effects.

Crack closure occurs when the fracture surfaces of a growing fatigue crack contact each other at some value of stress intensity greater than the minimum applied stress intensity,  $K_{min}$ . This premature closing of the crack during load reduction reduces the amplitude of stress intensity acting at the crack tip from the applied

value ( $\Delta K = K_{\max} - K_{\min}$ ) to some effective value ( $\Delta K_{\text{eff}} = K_{\max} - K_{\text{cl}}$ ), where  $K_{\text{cl}}$  is the stress intensity at which the crack is closed.<sup>32</sup>

The effect of closure raising threshold stress intensities is well documented.<sup>19,28,32-34</sup> Moreover, it has been found that when closure is allowed for, by the measurement of  $\Delta K_{\text{eff}}$  at threshold, or, the measurement of threshold stress intensity at high load ratio, microstructure has a minimal effect on thresholds in steels.<sup>19,34</sup> Threshold stress intensities at high load ratios and effective threshold stress intensities are typically in the range of 2 to 5 MPa $\sqrt{\text{m}}$  for a wide variety of steels.<sup>19,28,32,34</sup>

Following the ideas of Ritchie and Suresh, fatigue crack closure can be conveniently categorized into three types:<sup>32</sup> plasticity-induced crack closure, oxide-induced crack closure, and roughness-induced crack closure. Plasticity-induced crack closure was the first type of crack closure to be investigated.<sup>35</sup> In this case crack closure is caused by the monotonic tensile plastic strains that accompany fatigue crack growth. This mechanism of crack closure is most prevalent under conditions where the extent of plasticity is large, i.e., plane stress. Near-threshold fatigue crack growth occurs under conditions of plane strain. Hence, any plasticity-induced contribution to crack closure during near-threshold fatigue crack growth is necessarily small.<sup>32</sup>

Oxide-induced crack closure is caused by corrosion products that form near the crack tip during near-threshold fatigue crack growth.<sup>28,32</sup> Through the use of Auger spectroscopy it has been found that these corrosion products are metal oxides, and that they can have a thickness that is on the order of the crack tip opening displacement at threshold.<sup>28</sup>

Oxide-induced crack closure occurs when the corrosion products wedge the crack closed at a stress intensity above  $K_{min}$ . The concept of oxide-induced crack closure has proved to be invaluable in the explanation of environmental effects on fatigue thresholds.<sup>28</sup> In this study, the environment was identical for all of the fatigue crack growth tests. And, from visual inspection, albiet crude, it appeared that all of the steels tested exhibited similar extents of oxide formation. Therefore, the effect of oxide-induced crack closure on the fatigue thresholds measured in this study is assumed to be the same for all of the steels tested.

Roughness-induced crack closure is a result of a mismatch between the mating fatigue fracture surfaces. Crack closure occurs when the asperities of the mating fracture surfaces contact each other during load reduction at a stress intensity above  $K_{min}$ .<sup>32,33</sup> The observed correspondence between a coarse fracture surface and an increased threshold stress intensity in Fe/2Si/0.1C DFM(IQ) indicates that the closure effects manifested in this study are primarily due to a roughness-induced mechanism.

The importance of the large and abrupt changes in fracture surface profile towards the promotion of crack closure is made clear when the effect of Mode II displacements, which are known to be significant at threshold, are considered.<sup>36</sup> Mode II displacements augment crack closure by creating a lateral shift between the mating fracture surfaces. The incompatibility between fracture surfaces caused by a lateral shift is especially great when the fracture surfaces have large and abrupt changes in profile. Although the exact mechanism is uncertain, the origin of both the irregular fracture surface and the significant Mode II

displacements is thought to be a shear mode of crack growth in which crack tip plasticity and attendant crack extension are confined to a single active "flow band" that is inclined to the loading axis.<sup>33,37</sup> The shear mode of crack growth has been observed directly for short cracks,<sup>38,39</sup> with lengths on the order of microstructural features, and fractographic evidence indicates that it also operates for long cracks when the extent of plasticity is less than a grain size.<sup>33,40</sup>

The agreement found in the present work between the dimensions of near-threshold fracture surface features and the prior austenite grain size indicates that the prior austenite grain size can act as an important fracture unit for fatigue crack growth in DFM(IQ) steels. The coincidence of high threshold stress intensity and large prior austenite grain size in Fe/2Si/0.1C DFM(IQ) is consistent with the general, but not universal,<sup>41</sup> trend of increased grain size giving higher fatigue thresholds in steels.<sup>32,34,42,43</sup> The significance of the prior austenite grain size towards fatigue crack growth in Fe/2Si/0.1C DFM(IQ) was further demonstrated by the transition in crack growth rate and fracture surface topography that occurred when the monotonic plane strain plastic zone size was close to the prior austenite grain size. This observation is consistent with previous reports of markedly decreased crack closure when the maximum plastic zone size exceeds the grain size.<sup>44,45</sup>

However, a strong influence of prior austenite grain size was not realized in AISI 1018 DFM(IQ). Although the prior austenite grain size of AISI 1018 DFM(IQ) was less than half the prior austenite grain size of Fe/2Si/0.1C DFM(IQ), it was nine times larger than the ferrite grain size of AISI 1018 DFM(IA), and also four times larger than the monotonic

plane strain plastic zone size at threshold. Yet, both AISI 1018 DFM(IQ) and AISI 1018 DFM(IA) had nearly the same values of threshold stress intensity. If the differences in threshold stress intensity observed in the present work were primarily due to the extent of roughness-induced crack closure, then the low threshold stress intensity of AISI 1018 DFM(IQ) can be attributed to a smoother fracture surface, or, equivalently, a more direct crack path. Since it was found that the paths of the near-threshold fatigue cracks not dramatically altered when martensite particles were encountered, it is presumed that the distribution of martensite in AISI 1018 DFM(IQ) influenced crack tip plasticity such that the shear mode of crack growth was not promoted.

Near-threshold fatigue crack growth in other AISI 1018 duplex ferrite-martensite microstructures has been investigated. Suzuki and McEvily found that, for an equivalent, volume fraction of martensite, the microstructure consisting of ferrite encapsulated by martensite, DFM(B), exhibited a much higher value of threshold stress intensity than the microstructure consisting of martensite encapsulated by ferrite, DFM(A),  $14$  to  $18 \text{ MPa}\sqrt{\text{m}}$ \* versus  $8 \text{ MPa}\sqrt{\text{m}}$ , at a load ratio of  $0.05$ .<sup>18</sup> Subsequent work by Minakawa and McEvily revealed that the high value of threshold stress intensity for the DFM(B) microstructure was due to crack closure effects.<sup>19</sup> From fractographic examination, it was determined that the large closure effect measured for the DFM(B) microstructure was due to a roughness-induced mechanism. The fractographic features deemed responsible for the greater fracture surface roughness

---

\*  $18 \text{ MPa}\sqrt{\text{m}}$  was presented as data.  $14 \text{ MPa}\sqrt{\text{m}}$  was reported in a note added in proof. The discrepancy was unexplained.

were planar, transgranular, facets called "shear facets." The facets had the distinct appearance of being formed by a shear mechanism of crack growth. It can be noted that the "steps" on the fracture surface feature of Fe/2Si/0.1C DFM(IQ), shown in Fig. (13c), have some resemblance to the reported "shear facets." Hence, it appears that any duplex ferrite-martensite microstructure that promotes the formation of rough fracture surfaces can have a high threshold stress intensity because of roughness-induced crack closure. A shear mode of crack growth appears to be instrumental in both creating the rough fracture surface and enhancing crack closure through Mode II displacement.



## V. CONCLUSIONS

Based on a study of tensile and fatigue crack growth behavior in AISI 1018 and Fe/2Si/0.1C steels with duplex ferrite-martensite (DFM) microstructures, the following conclusions were made.

1. The tensile deformation behavior of AISI 1018 DFM steels, especially elongation to failure, was sensitive to both the distribution and volume fraction of martensite. The elongation to tensile failure was drastically reduced when sizes of the ferrite and martensite particles were increased.

2. Threshold stress intensities for fatigue crack growth in AISI 1018 DFM were largely unaffected by changes in the distribution and volume fraction of martensite.

3. The threshold stress intensity for fatigue crack growth in Fe/2Si/0.1C DFM(IQ) was considerably greater than that in AISI 1018 DFM(IQ) at comparable yield strength. The higher threshold of Fe/2Si/0.1C DFM(IQ) appeared to be due to crack closure that was induced fracture surface roughness. The rough fracture surface was presumably promoted by a large prior austenite grain size and a favorable distribution of martensite.

4. Fatigue crack growth rates were greater for AISI 1018 DFM(IA) than AISI 1018 DFM(IQ) in the range of  $10^{-5}$  to  $10^{-3}$  mm/cycle due to the occurrence of extensive cleavage fracture in ferrite. This cleavage fracture appears to be a result of large martensite particles restricting plastic flow of ferrite.

## ACKNOWLEDGEMENTS

The author extends his appreciation and gratitude to Professor Gareth Thomas for his guidance and encouragement throughout the course of this investigation. The expert advice given by Professor R. O. Ritchie is also greatly appreciated. Special thanks are also due to Professor I. Finnie for reviewing this manuscript.

The author would also like to thank all members of Professor Thomas' steel group for their helpful discussions and advice. The support of the technical staff of the Materials and Molecular Research Division of the Lawrence Berkeley Laboratory was invaluable. Thanks are also due to Madeleine Penton for typing this manuscript.

This work was supported by the Director, Office of Energy Research, Office of Basic Energy Sciences, Division of Materials Science of the U.S. Department of Energy under Contract number DE-AC03-76SF 00098.

## REFERENCES

1. Jayoung Koo, "Design of Duplex Low Carbon Steels for Improved Strength: Weight Applications," Ph.D. Thesis, University of California, Berkeley, LBL-6657, August 1977.
2. G. Thomas and J. Y. Koo, "Developments in Strong, Ductile Duplex Ferrite-Martensite Steels," Structure and Properties of Dual-Phase Steels, R. A. Kot and J. W. Morris, eds., AIME, New York, N.Y. (1979), p. 183.
3. W. S. Owen, Fifth Harold Moore Lecture, "Can a Simple Heat Treatment Help to Save Detroit?" Metals Technology 7 (1980), 1-13.
4. Nack-Joon Kim, "Design of Dual Phase Fe/Mn/C Steel for Low Temperature Application," Ph.D. Thesis, University of California, Berkeley, LBL-12661 (1981).
5. J. Y. Koo and G. Thomas, "Thermal Cycling Treatments and Microstructures for Improved Properties of Fe-0.12%C-0.5%Mn Steels," Mat. Sci. and Eng. 24 (1976), 187.
6. J. Y. Koo, M. J. Young, and G. Thomas, "On the Law of Mixtures in Dual-Phase Steels," Met. Trans. A 11A (1980), 852.
7. N. J. Kim and G. Thomas, "Effects of Morphology on the Mechanical Behavior of a Dual-Phase Fe/2Si/0.1C Steel," Met. Trans. A 12A (1981), 483.
8. P. K. Costello, "Design of Duplex Low Carbon Steels with Carbide Forming Elements," M.S. Thesis, University of California, Berkeley, LBL-8628 (Dec. 1978).

9. T. J. O'Neill, J. Y. Koo, and G. Thomas, "Microstructure and Properties of Dual Phase Steels Containing Silicon, Aluminum, and Molybdenum," submitted to Met. Trans., Nov. 1980.
10. J. S. Gau, "Mechanical Properties and Microstructure of a Low Carbon Steel with Nb," M.S. Thesis, University of California, Berkeley, LBL-12058, April 1981.
11. Alvin Nakagawa, J. Y. Koo, and G. Thomas, "Effect of Vanadium on Structure-Property Relations of Dual Phase Fe/Mn/Si/0.1C Steels," Met. Trans. A 12A (1981), 1965-1971.
12. R. G. Davies, "The Deformation Behavior of a Vanadium-Strengthened Dual Phase Steel," Met. Trans. A 9A (1978), 41-52.
13. A. M. Sherman and R. G. Davies, "The Effect of Martensite Content on the Fatigue of a Dual-Phase Steel," Int. J. Fatigue 3 (1981), 36-40.
14. T. Kunio and K. Yamada, "Microstructural Aspects of the Threshold Condition for Nonpropagating Fatigue Cracks in Martensitic-Ferritic Structures," in Fatigue Mechanisms, ASTM STP 675 (1978), p. 342.
15. T. Kunio et al., "The Influence of Threshold Behavior of Micro-crack on the Endurance Limit of Dual Phase Steel," Proceedings from the International Symposium on Fatigue Thresholds, Stockholm, Sweden, 1-3 June 1981, Vol. 1.
16. P. C. Paris, Fatigue, an Interdisciplinary Approach, Proceedings of the 10th Sagamore Army Materials Research Conference, Syracuse University Press (1964), p. 107.
17. J. R. Rice, "Mechanics of Crack Tip Deformation and Extension by Fatigue," ASTM 415, Am. Soc. Testing Mats. (1967), p. 247.

18. H. Suzuki and A. J. McEvily, "Microstructural Effects on Fatigue Crack Growth in a Low Carbon Steel," *Met. Trans. A* 10A (1979), 475-481.
19. K. Minakawa, Y. Matsuo, and A. J. McEvily, "The Influence of a Duplex Microstructure in Steels on Fatigue Crack Growth in the Near-Threshold Region," *Met. Trans. A* 13A (1982), 439-445.
20. R. O. Ritchie, "Crack Growth Monitoring: Some Considerations on the Electric Potential Method," Technical Report, Department of Metallurgy and Materials Science, University of Cambridge, Jan. 1972.
21. R. O. Ritchie and K. J. Bathe, "On the Calibration of the Electrical Potential Technique for Monitoring Crack Growth Using Finite Element Methods," *Int. Journ. of Fracture* 15 (1979), 47-55.
22. J. F. Knott, Fundamentals of Fracture Mechanics, Butterworths, London (1973), p. 67.
23. D. M. Tracey, "Finite Element Solutions for Crack Tip Behavior in Small-Scale Yielding," *Journ. Eng. Matl. Tech.* (1976), 146-151.
24. E. E. Underwood, "Applications of Quantitative Metallography," in ASM Metals Handbook, Vol. 8 (1961), p. 37.
25. J. Becker and E. Hornbogen, "Microscopic Analysis of the Formation of Dual Phase Steels," in *Proceedings of AIME Annual Meeting*, Feb. 19-21, 1979, New Orleans, LA.
26. C. A. Apple, R. N. Caron, and G. Krauss, "Packet Microstructure in Fe-0.2 pct. Martensite," *Met. Trans.* 5 (1974), 593-599.
27. M. J. Young, "Heat Treatment and Characterization of Duplex 1010 and 1020 Steels," M.S. Thesis, University of California, Berkeley, LBL-6620 (Nov. 1977).

28. S. Suresh, G. F. Zaminski, and R. O. Ritchie, "Oxide-Induced Crack Closure: An Explanation for Near-Threshold Corrosion Fatigue Behavior," *Met. Trans. A* 12A (1981), 1435-1443.
29. R. J. Bucci, "Effects of Residual Stress on Fatigue Crack Growth Rate Measurements," *ASTM STP* 743 (1981), pp. 28-47.
30. R. O. Ritchie and J. F. Knott, "Micro Cleavage Cracking During Fatigue Crack Propagation in Low Strength Steel," *Mat. Sci. and Eng.* 14 (1974), 7-14.
31. T. C. Lindley, C. E. Richards, and R. O. Ritchie, "The Mechanics and Mechanisms of Fatigue Crack Growth in Metals," *Metallurgia and Metal Forming* 43 (1976), 268-280.
32. R. O. Ritchie and S. Suresh, "Some Considerations on Fatigue Crack Closure at Near-Threshold Stress Intensities due to Fracture Surface Morphology," *Met. Trans. A* 13A (1982), 937-940.
33. K. Minakawa and A. J. McEvily, "On Crack Closure in the Near-Threshold Region," *Scripta Met.* 15 (1981), 633-636.
34. G. T. Gray, III, A. W. Thompson, J. C. Williams, and D. H. Stone, "Influence of Microstructure on Fatigue Crack Growth Behavior in Fully Pearlitic Steels," *Proceedings from the International Symposium on Fatigue Thresholds, Stockholm, Sweden, 1-3 June 1981, Vol. 2.*
35. Elber, "Fatigue Crack Closure Under Cyclic Tension," *Engineering Fracture Mechanics* 2 (1970), 37-45.
36. S. Suresh and R. O. Ritchie, "A Geometric Model for Fatigue Crack Closure Induced by Fracture Surface Roughness," *Met. Trans. A* 13A (1982), in press.

37. B. Tomkins, "Role of Mechanics in Corrosion Fatigue," *Metal Science* 13 (1979), 387-395.
38. A. J. McEvily and R. C. Boettner, "On Fatigue Crack Propagation in F.C.C. Metals," *Acta Met.* 11 (1963), 725-743.
39. Cambell Laird, "The Influence of Metallurgical Structure on the Mechanisms of Fatigue Crack Propagation," *Fatigue Crack Propagation ASTM STP 415* (1966), 131-180.
40. A. Otsuka, K. Mori, and T. Miyata, "The Condition of Fatigue Crack Growth in Mixed Mode Condition," *Eng. Frac. Mech.* 7 (1975), 429-439.
41. M. F. Carlson and R. O. Ritchie, "On the Effect of Prior Austenite Grain Size on Near-Threshold Fatigue Crack Growth," *Scripta Met.* 11 (1977), 1113-1118.
42. J. Masounave and J. P. Bailon, "Effect of Grain Size on the Threshold Stress Intensity Factor in Fatigue of a Ferritic Steel," *Scripta Met.* 10 (1976), 165-170.
43. J. P. Benson, "Influence of Grain Size and Yield Strength on Threshold Fatigue Behavior of Low-Alloy Steel," *Metal Science* (1979), 535-539.
44. R. J. Cooke and C. J. Beevers, "The Effect of Load Ratio on the Threshold Stresses for Fatigue Crack Growth in Medium Carbon Steels," *Eng. Fract. Mech.* 5 (1973), 1061-1071.
45. R. J. Asaro, L. Hermann, and J. M. Baik, "Transitions in Fatigue Crack Closure in 2048 Aluminum," *Met. Trans. A* 12A (1981), 1133-1135.

TABLE I

Specimen Designation*	Martensite Volume Fraction (%)	Austenitizing Temperature (°C)	$\alpha+\gamma$ Annealing Temperature (°C)
AISI 1018 DFM(IA)	37	1100	735
AISI 1018 DFM(IQ)	35	1100	735
AISI 1018 DFM(IA)	48	1100	755
AISI 1018 DFM(IQ)	46	1100	755
Fe/2Si/0.1C DFM(IQ)	41	1150	990

\* (IA) = intercritical anneal heat treatment

(IQ) = intermediate quench heat treatment

TABLE II

Specimen Designation	Martensite Volume Fraction (%)	Ferrite Particle Size $\bar{L}_\alpha$ (microns)	Martensite Particle Size $\bar{L}_\gamma$ (microns)	Martensite Connectivity $\psi$ (%)
AISI 1018 DFM(IA)	37	9	6	88
AISI 1018 DFM(IQ)*	35	4	2	>95
AISI 1018 DFM(IA)	48	9	5	95
AISI 1018 DFM(IQ)*	46	1	3	>95
AISI 1018 (as received)	--	12	5	--
Fe/2Si/0.1C DFM(IQ) <sup>†</sup>	41	8	3	>95

\* Prior austenite grain size  $\sim 80 \mu\text{m}$

<sup>†</sup> Prior austenite grain size  $\sim 180 \mu\text{m}$



TABLE III

Specimen Designation	Vol.% Martensite	Yield Strength		U.T.S.		$\epsilon_u$ %*		$\epsilon_T$ %	
		(MPa)	(ksi)	(MPa)	(ksi)				
AISI 1018 DFM(IA)	37	536 <sup>+21</sup> -12	77.9 <sup>+3.0</sup> -1.7	843 <sup>+32</sup> -20	122.4 <sup>+4.6</sup> -2.9	6.8 <sup>+0.6</sup> -0.4	9.4 <sup>+1.6</sup> -1.6		
AISI 1018 DFM(IQ)	35	452 <sup>+21</sup> -21	65.6 <sup>+3.1</sup> -3.0	784 <sup>+42</sup> -34	113.8 <sup>+6.1</sup> -5.0	13.7 <sup>+0.7</sup> -0.8	19.8 <sup>+2.0</sup> -1.0		
AISI 1018 DFM(IA)	48	668 <sup>+40</sup> -20	97.0 <sup>+5.8</sup> -3.5	971 <sup>+10.3</sup> -18.6	140.9 <sup>+1.5</sup> -2.7	6.4 <sup>+0.5</sup> -0.4	9.0 <sup>+0.4</sup> -1.2		
AISI 1018 DFM(IQ)	46	546 <sup>+8</sup> -8	79.3 <sup>+1.2</sup> -1.1	904 <sup>+32</sup> -26	131.2 <sup>+4.6</sup> -3.8	10.2 <sup>+0.7</sup> -1.0	13.6 <sup>+1.7</sup> -1.1		
Fe/2Si/0.1C DFM(IQ)	41	508 <sup>+11</sup> -14	73.7 <sup>+1.6</sup> -2.1	796 <sup>+25</sup> -15	115.5 <sup>+3.7</sup> -2.2	13.6 <sup>+0.8</sup> -0.8	20.6 <sup>+0.5</sup> -0.3		
AISI 1018 (martensitic)	100	1067 <sup>+12</sup> -15	154.8 <sup>+1.7</sup> -2.2	1289 <sup>+3</sup> -2	187.1 <sup>+0.4</sup> -0.3	3.5 <sup>+0.2</sup> -0.2	11.8 <sup>+0.7</sup> -0.4		
AISI 1018 DFM(IA) (4 hour anneal)	48	655 <sup>+13</sup> -13	95.0 <sup>+1.9</sup> -1.9	980 <sup>+4</sup> -4	142.2 <sup>+0.6</sup> -0.6	6.3 <sup>+0.4</sup> -0.4	8.4 <sup>+0.6</sup> -0.6		
AISI 1018 DFM(IQ) (4 hour anneal)	46	544 <sup>+21</sup> -21	79.0 <sup>+3.0</sup> -3.0	938 <sup>+1.6</sup> -1.6	136.1 <sup>+1.1</sup> -1.1	9.8 <sup>+0.4</sup> -0.4	12.5 <sup>+0.0</sup> -0.0		

\* One inch gage length

TABLE IV

Specimen Designation	Martensite Vol. %	$\Delta K_o$		Approximate Paris <sup>*</sup> Law Exponent, m	Number of Specimens Tested
		(MPa $\sqrt{m}$ )	(ksi $\sqrt{m}$ )		
AISI 1018 DFM(IA)	37	9.2 $\begin{smallmatrix} +0.8 \\ -0.5 \end{smallmatrix}$	8.4 $\begin{smallmatrix} +0.7 \\ -0.5 \end{smallmatrix}$	5.6	4
AISI 1018 DFM(IQ)	35	9.7 $\begin{smallmatrix} +1.2 \\ -1.7 \end{smallmatrix}$	8.8 $\begin{smallmatrix} +1.1 \\ -1.5 \end{smallmatrix}$	4.4	4
AISI 1018 DFM(IA)	48	9.3 $\begin{smallmatrix} +0.3 \\ -0.3 \end{smallmatrix}$	8.5 $\begin{smallmatrix} +0.3 \\ -0.3 \end{smallmatrix}$	5.4	3
AISI 1018 DFM(IQ)	46	9.6 $\begin{smallmatrix} +0.0 \\ -0.0 \end{smallmatrix}$	8.7 $\begin{smallmatrix} +0.0 \\ -0.0 \end{smallmatrix}$	4.6	3
Fe/2Si/0.1C DFM(IQ)	41	15.8 $\begin{smallmatrix} +1.2 \\ -0.8 \end{smallmatrix}$	14.4 $\begin{smallmatrix} +1.1 \\ -0.7 \end{smallmatrix}$	9.9/4.5 !	3

\*  $\frac{da}{dN} = C \Delta K^m$  m was estimated by drawing the best straight line through  $\log \frac{da}{dN}$  vs.  $\log \Delta K$  data points in the range  $10^{-5}$  mm/cycle  $< \frac{da}{dN} < 10^{-3}$  mm/cycle; C is a constant.

! 9.9 applies for  $10^{-5}$  mm/cycle  $< \frac{da}{dN} < 10^{-4}$  mm/cycle; 4.5 applies for  $\frac{da}{dN} > 10^{-4}$  mm/cycle.

## FIGURE CAPTIONS

- Fig. (1). Drawings of (a) ASTM specification E8-69 flat tensile specimen, and (b) compact specimen.
- Fig. (2). Optical Micrographs of AISI 1018, (a) as received, (b) martensitic, (c) DFM intercritical anneal, 48 vol.% martensite, and (c) DFM intermediate quench, 46 vol.% martensite.
- Fig. (3). SEM micrographs of AISI 1018 DFM, (a) intercritical anneal, 48 vol.% martensite and (b) intermediate quench, 46 vol.% martensite.
- Fig. (4). Optical micrograph of Fe/2Si/0.1C DFM(IQ), 41 vol.% martensite, containing a near-threshold fatigue crack. The direction of crack growth was from left to right. The arrow points to the crack tip.
- Fig. (5). SEM micrograph of Fe/2Si/0.1C DFM(IQ), 41 vol.% martensite.
- Fig. (6). Transmission electron micrographs of AISI 1018 DFM(IQ).
- Fig. (7). Monotonic stress-strain curves for AISI 1018 DFM(IA), 37 vol.% martensite and AISI 1018 DFM(IQ), 35 vol.% martensite.
- Fig. (8). Plots of tensile properties versus martensite volume fraction.
- Fig. (9). Fatigue crack growth curves for AISI 1018 DFM and Fe/2Si/0.1C DFM, all at ~40 vol.% martensite.

Fig. (10). SEM fractographs of tensile fracture in (a) AISI 1018 DFM (IA), 37 vol.% martensite and (b) AISI 1018 DFM(IQ), 35 vol.% martensite. (c) is an SEM fractograph of a taper section of tensile fracture in AISI 1018 DFM(IA), 37 vol.% martensite. The polished and etched surface is at the bottom of the photograph.

Fig. (11). Low magnification ( $\sim 5X$ ) optical fractographs of the fatigue fracture surfaces of (a) AISI 1018 DFM(IA), 37 vol.% martensite, (b) AISI 1018 DFM(IQ), 35 vol.% martensite, and (c) Fe/2Si/0.1C DFM(IQ), 41 vol.% martensite. The crack growth direction is from left to right. The arrow in (c) indicates the position at which a change in fracture surface roughness occurred.

Fig. (12). SEM fractographs of near-threshold fatigue fracture in (a) AISI 1018 DFM(IA), 37 vol.% martensite, (b) AISI 1018 DFM(IQ), 35 vol.% martensite, and (c) Fe/2Si/0.1C DFM(IQ), 41 vol.% martensite. The crack growth direction is from left to right.

Fig. (13). (a) is a SEM fractograph of near-threshold fatigue fracture in AISI 1018 DFM(IQ). (b) is a higher magnification fractograph of the region outlined in (a). (c) is a SEM fractograph of near-threshold fatigue fracture in Fe/2Si/0.1C DFM(IQ). (d) is a higher magnification fractograph of the region shown in (c). The crack growth direction is from left to right.

- Fig. (14). (a) is an optical micrograph of a near-threshold fatigue crack in AISI 1018 DFM(IA), 37 vol.% martensite. (b) is a higher magnification SEM micrograph of the same crack. The crack growth direction is from left to right. The arrows point to identical positions of crack path.
- Fig. (15). Optical micrographs of near-threshold fatigue cracks in (a) AISI 1018 DFM(IQ) and (b) Fe/2Si/0.1C DFM(IQ). The specimens were tempered and etched to reveal prior austenite grain boundaries. The crack growth direction is from left to right.
- Fig. (16). Plot of percent cleavage fracture versus  $\Delta K$  for AISI 1018 DFM(IA), 37 vol.% martensite.
- Fig. (17). SEM fractographs of mid-growth range fatigue fracture in (a) AISI 1018 DFM(IA), 48 vol.% martensite,  $\Delta K \cong 28 \text{ MPa}\sqrt{\text{m}}$ , (b) AISI 1018 DFM(IQ), 46 vol.% martensite,  $\Delta K \cong 28 \text{ MPa}\sqrt{\text{m}}$ . (c) and (d) are SEM fractographs of taper sections of fatigue fracture in the structures just described, (c) DFM(IA) and (d) DFM(IQ). The polished and etched surfaces take up the bottom half of the photographs. The crack growth direction is from left to right.
- Fig. (18). SEM fractograph of mid-growth range fatigue fracture in Fe/2Si/0.1C DFM(IQ). A distinct change in fracture surface topography can be seen in the middle of the figure ( $\Delta K \cong 33 \text{ MPa}\sqrt{\text{m}}$ ). The crack growth direction is from left to right.

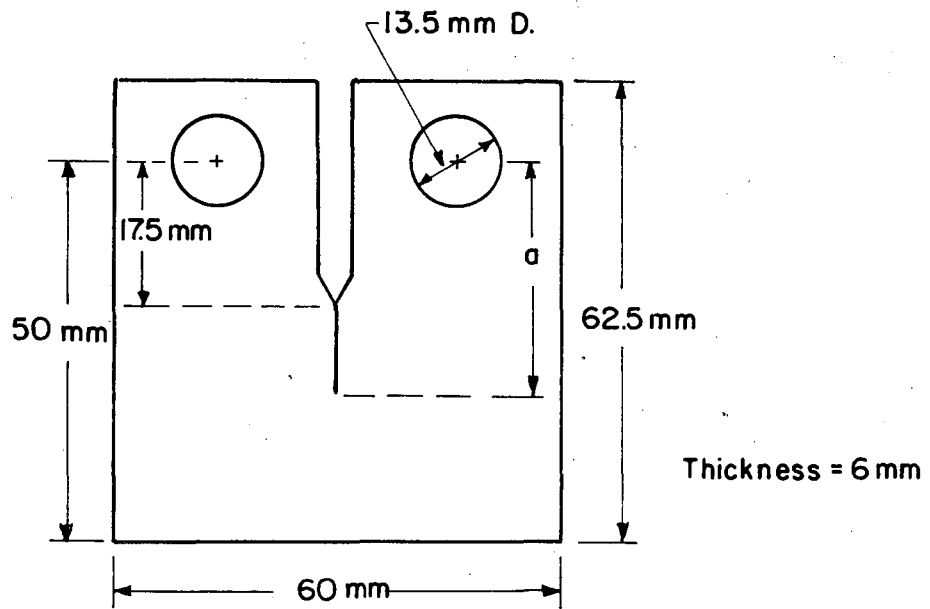
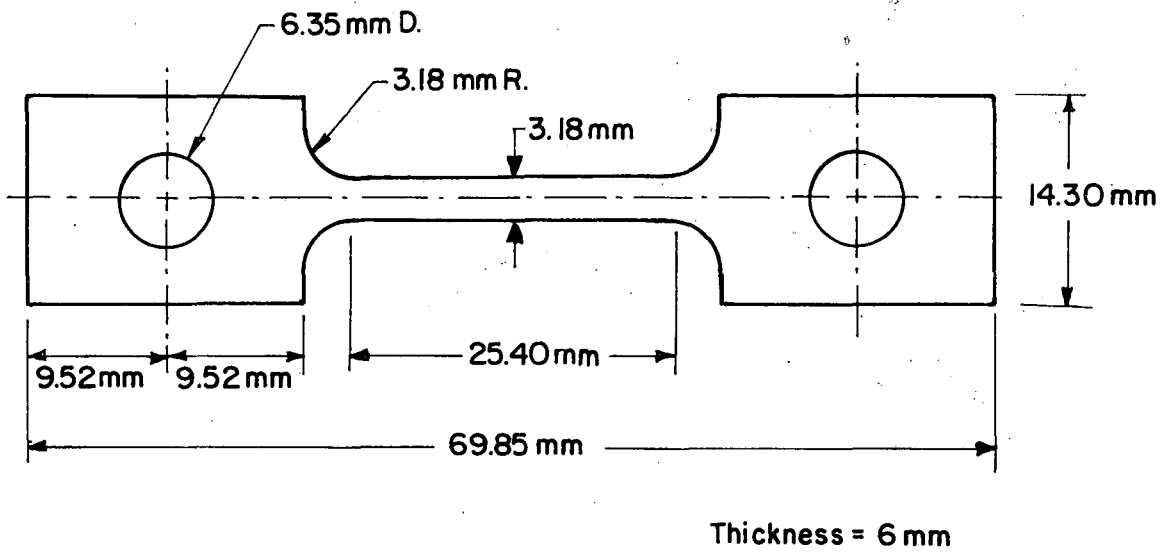


Fig. (1)

XBL 823-5355



Fig. (2)

XBB 821-1130

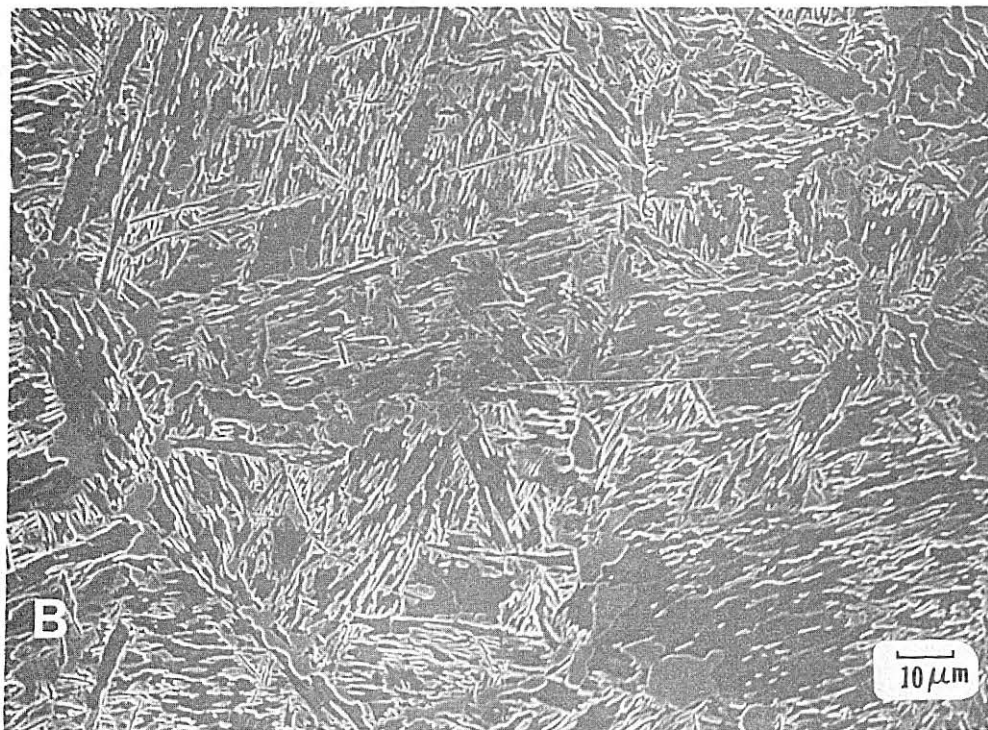
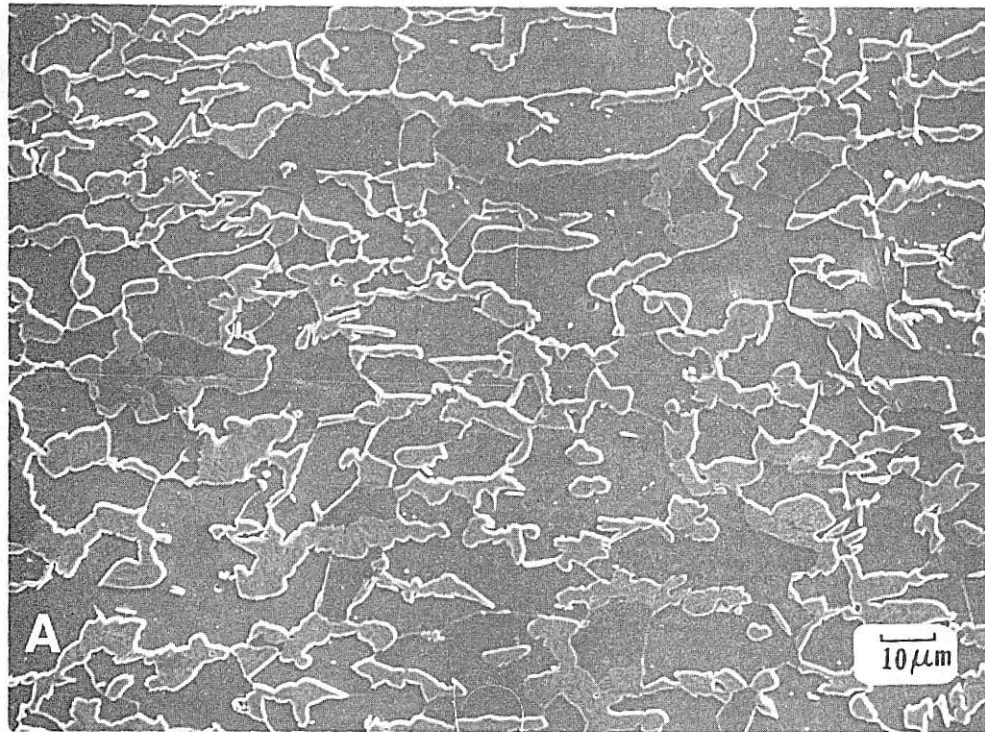


Fig. (3)

XBB 821-804



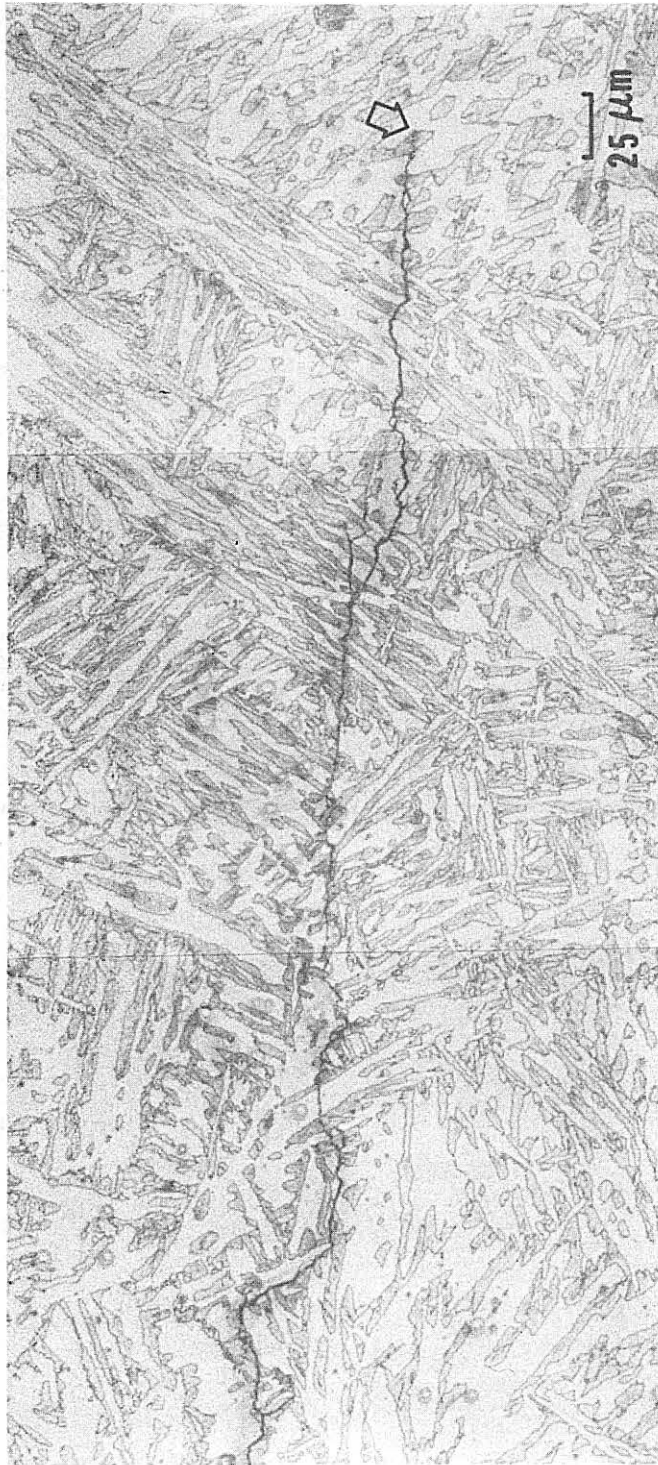


Fig. (4)

XBB 821-1131

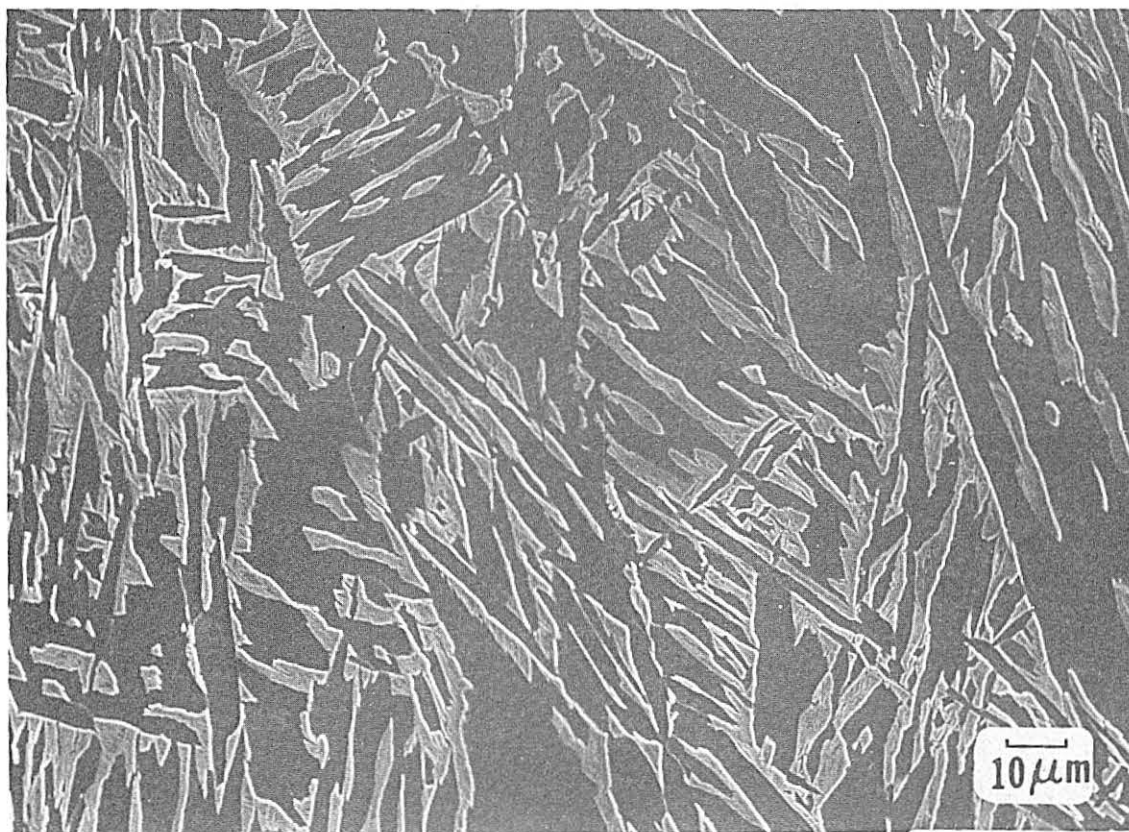


Fig. (5)

XBB 824-4513

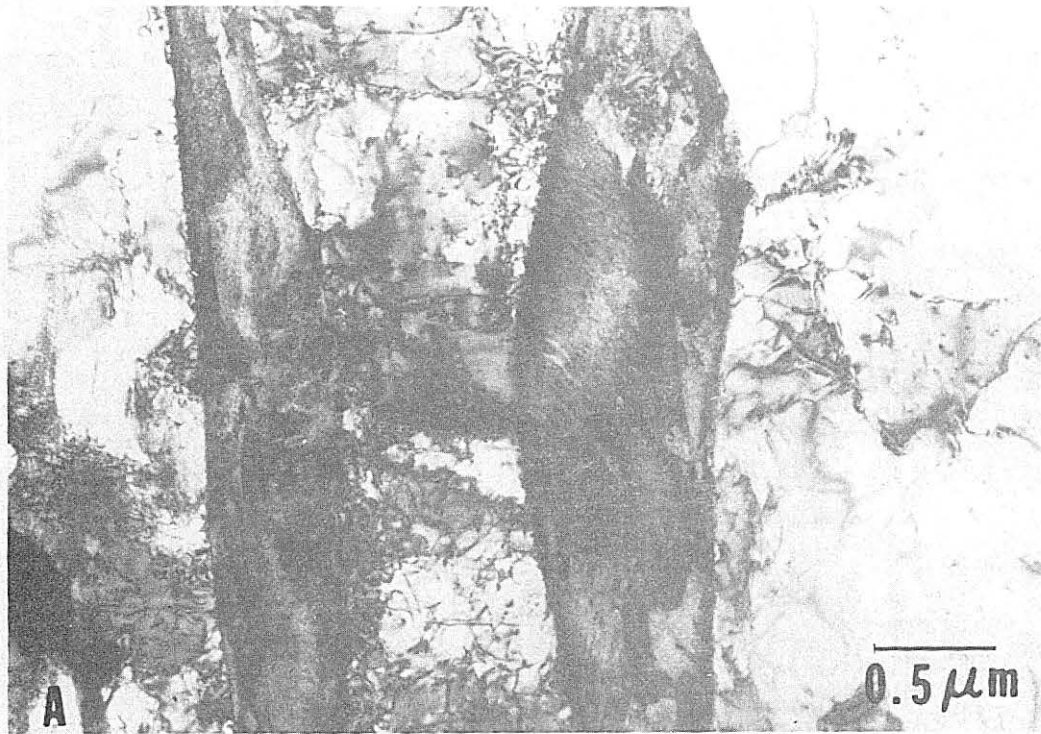
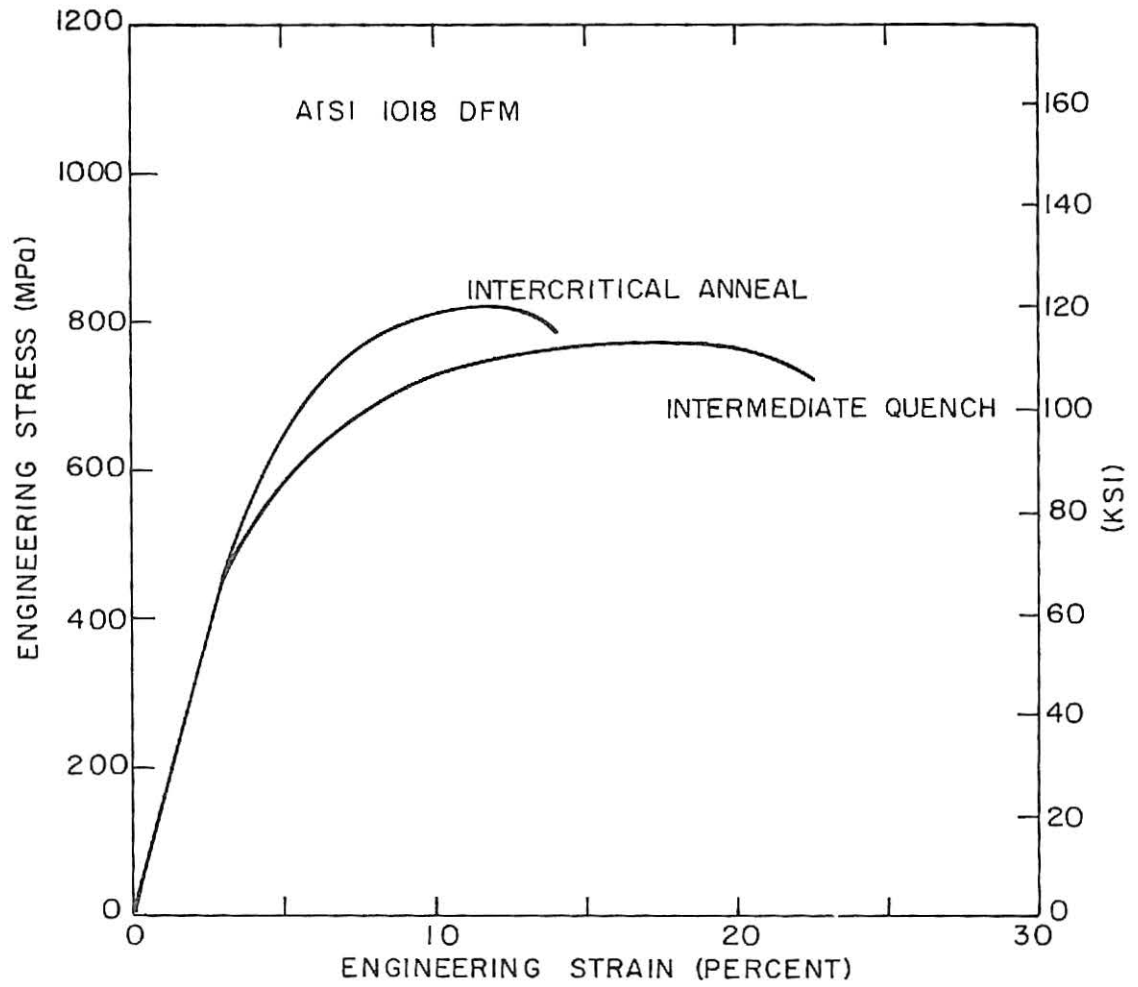


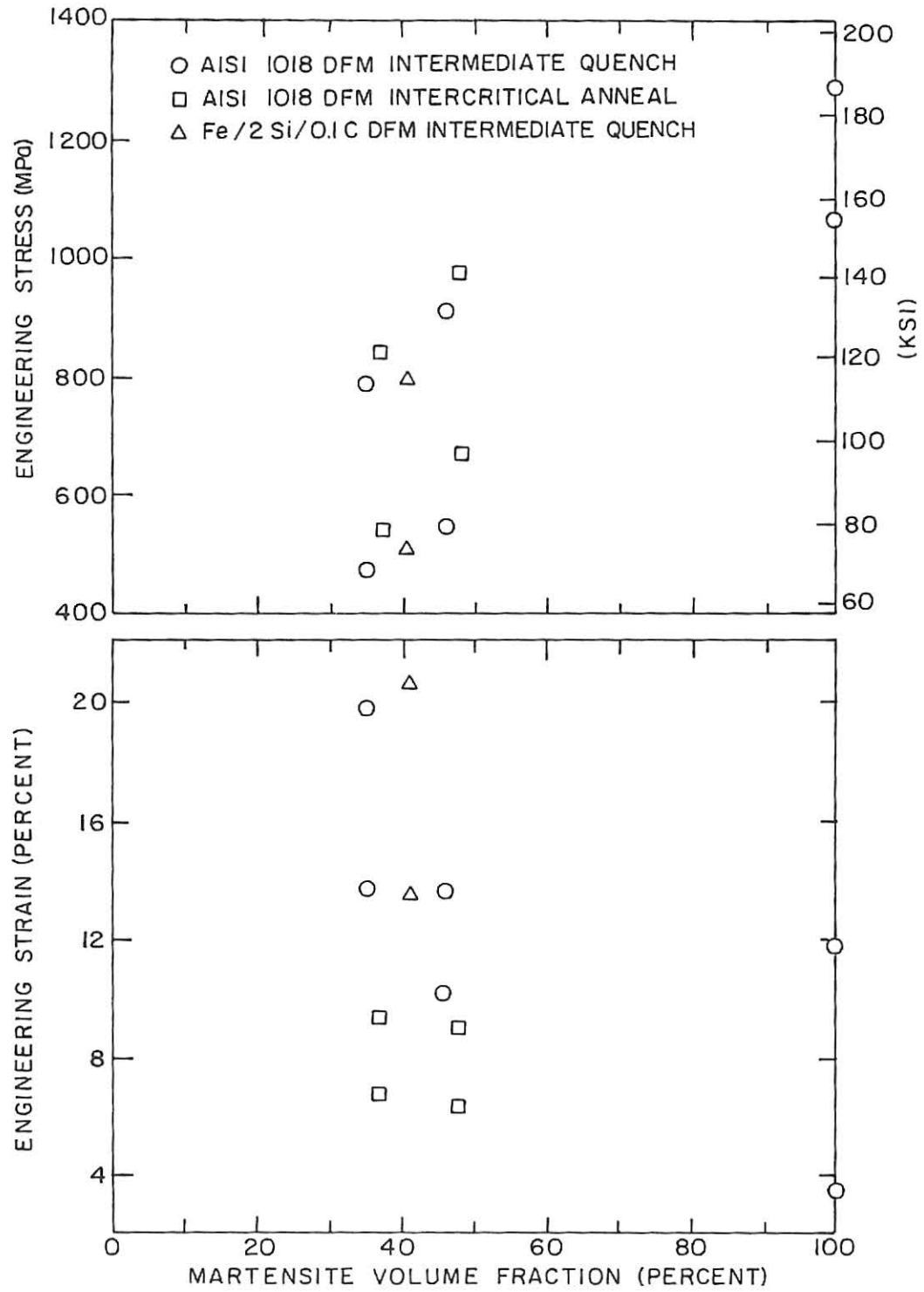
Fig. (6)

XBB 826-5292



XBL 822-5154

Fig. (7)



XBL 822-5153

Fig. (8)

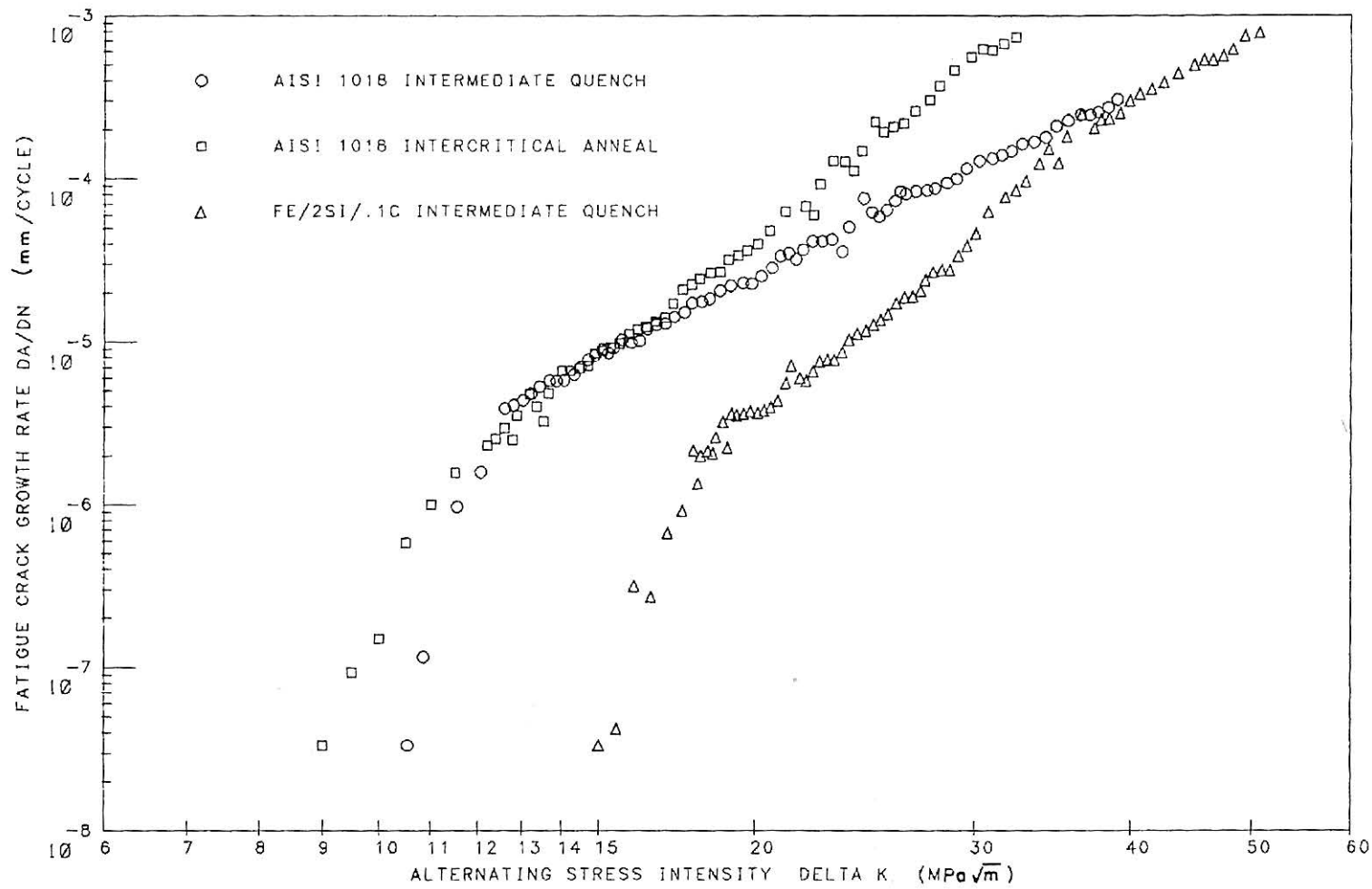


Fig. (9)

XBL 8112-12949

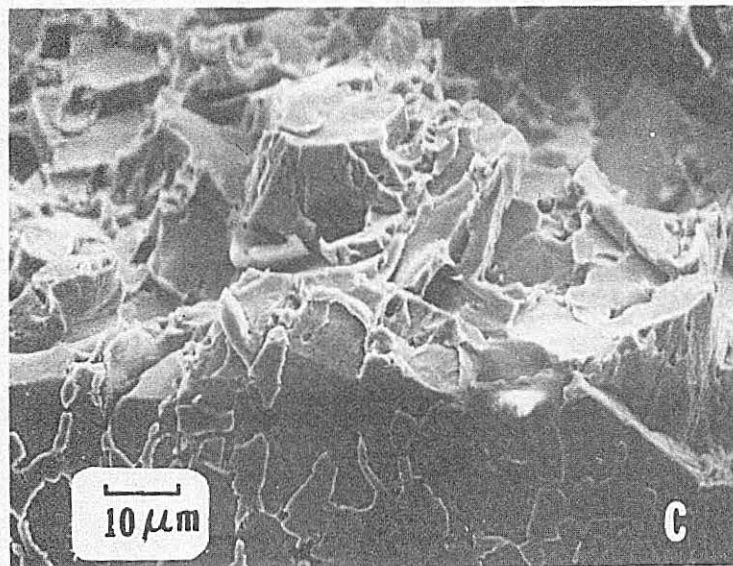
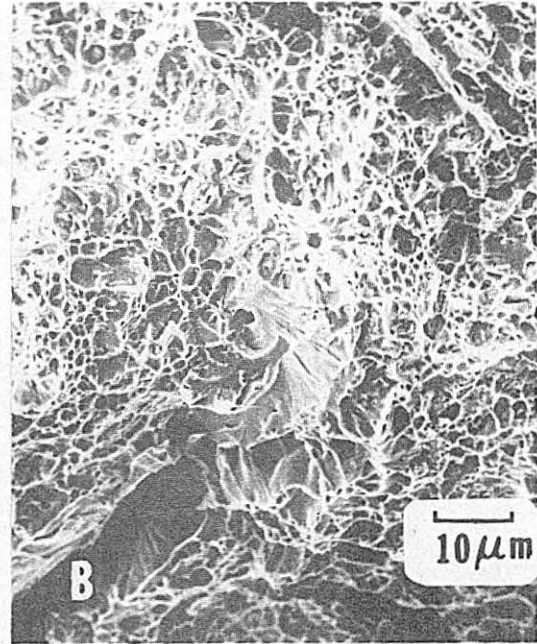
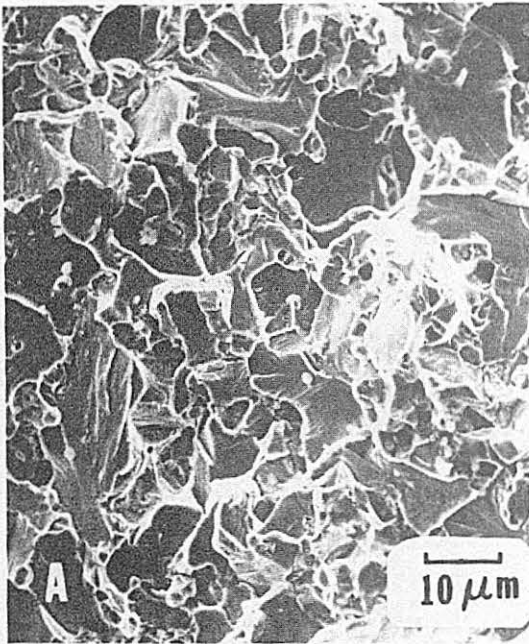


Fig. (10)

XBB 821-806



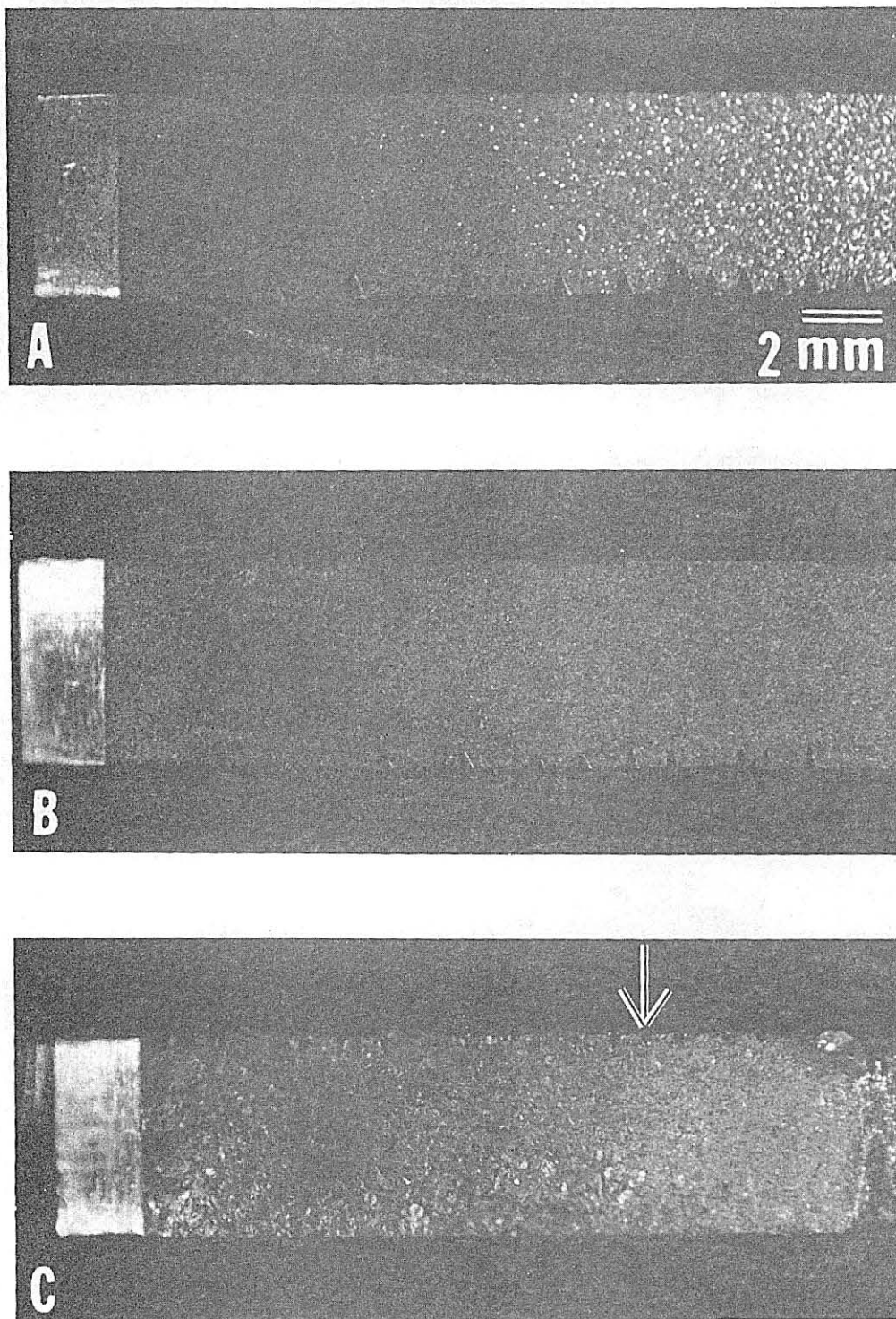


Fig. (11)

XBB 825-4285



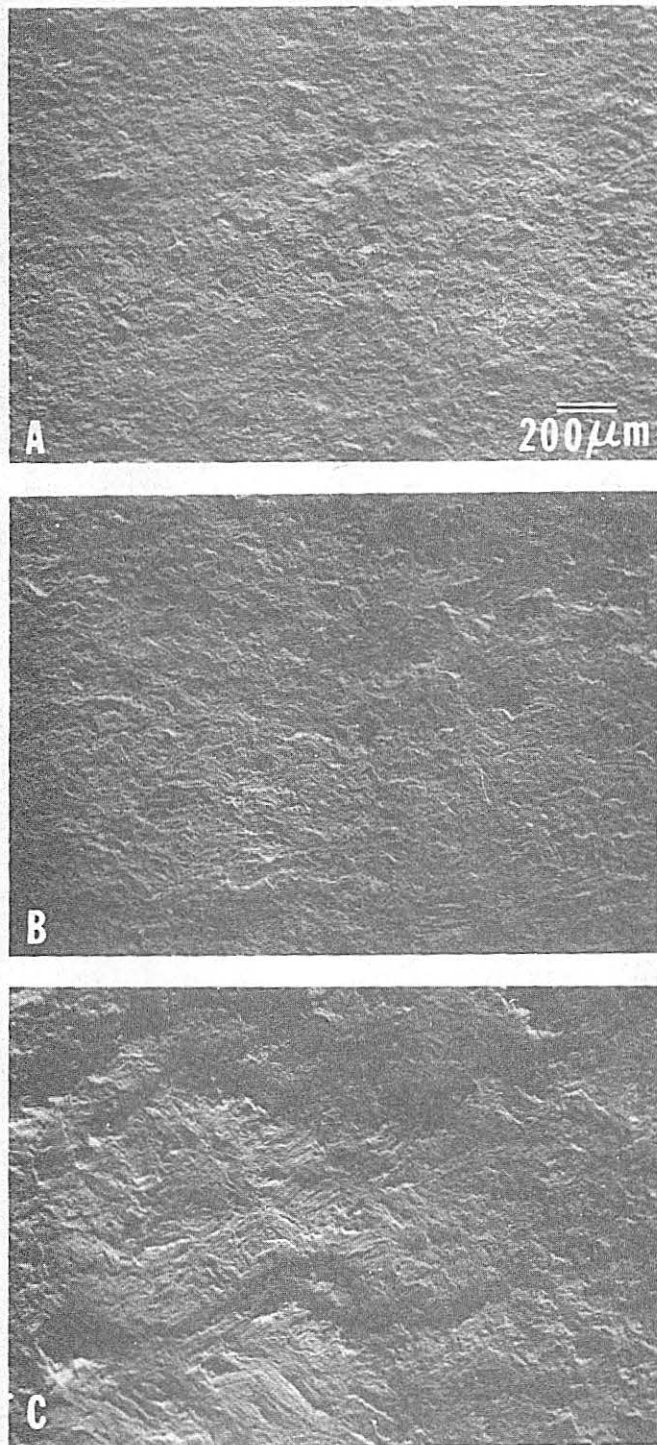


Fig. (12)

XBB 825-4287

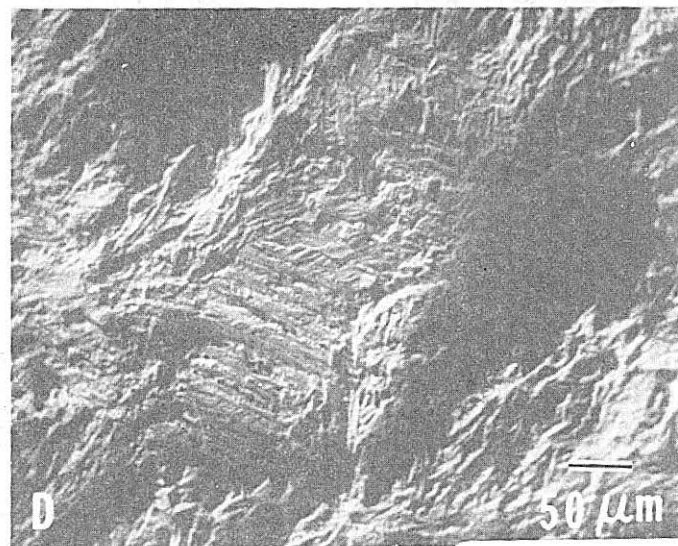
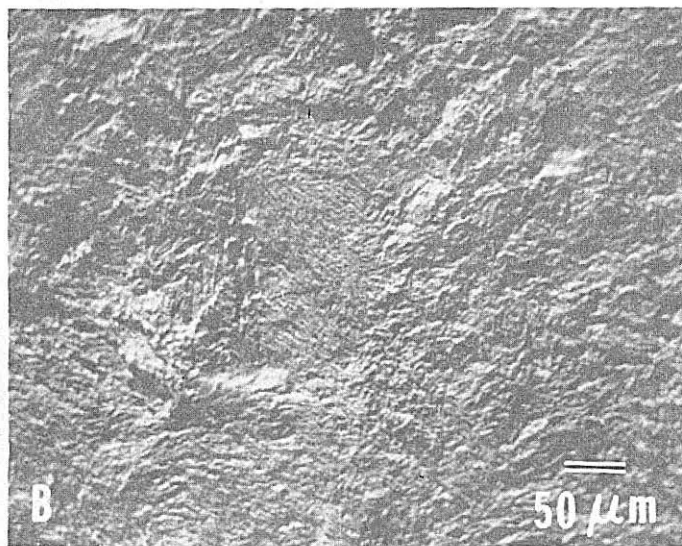
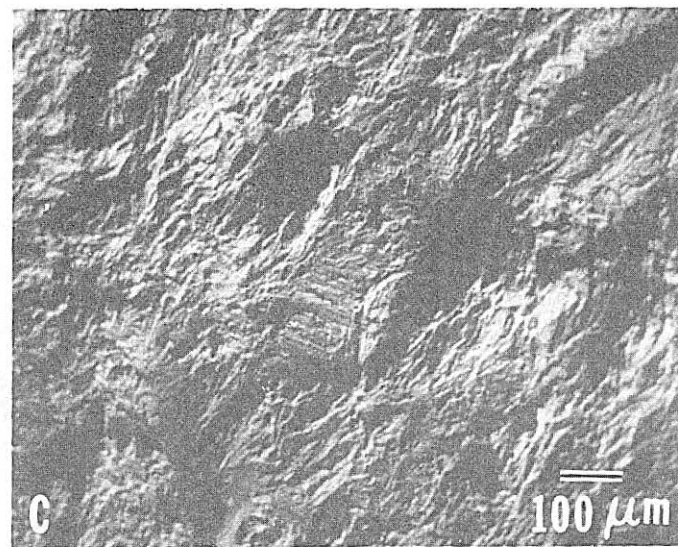
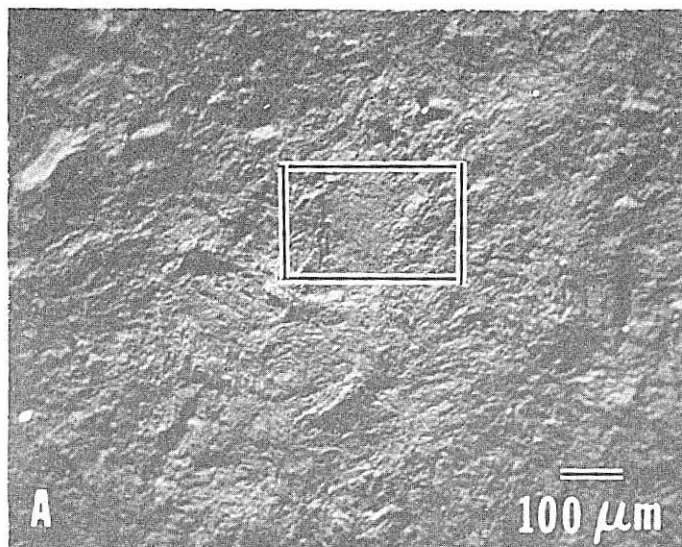


Fig. (13)

XBB 825-4283

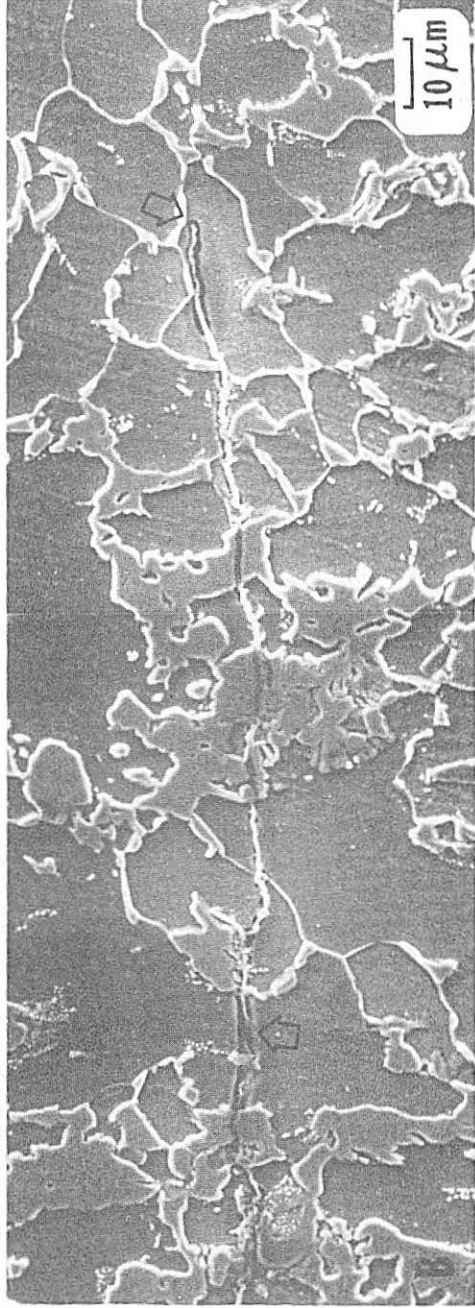
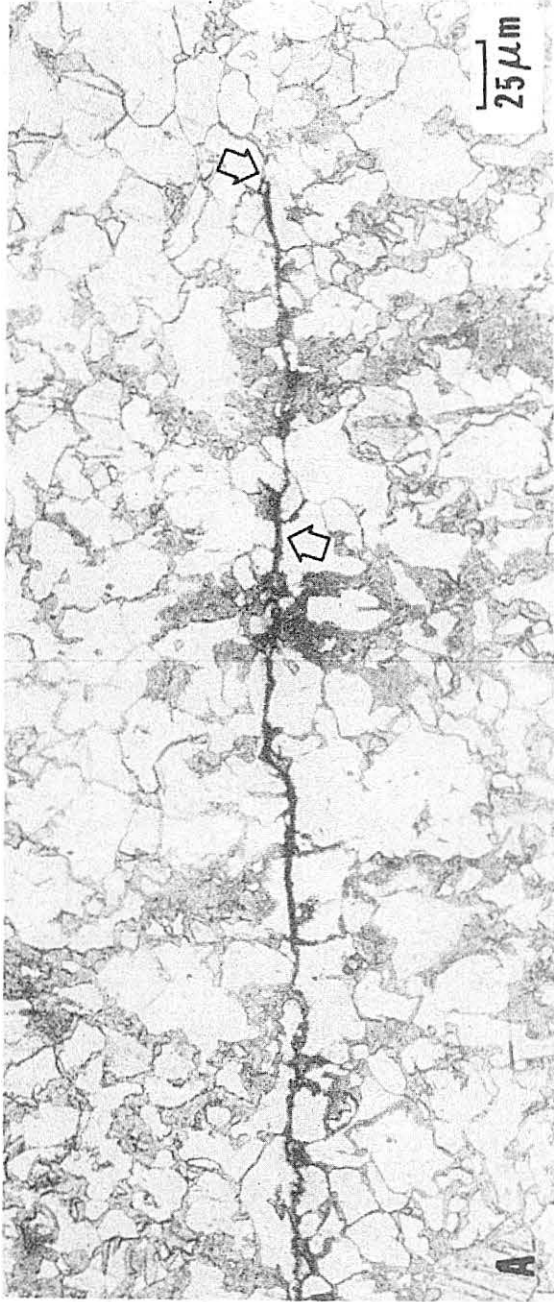


Fig. (14)

XBB 821-1132

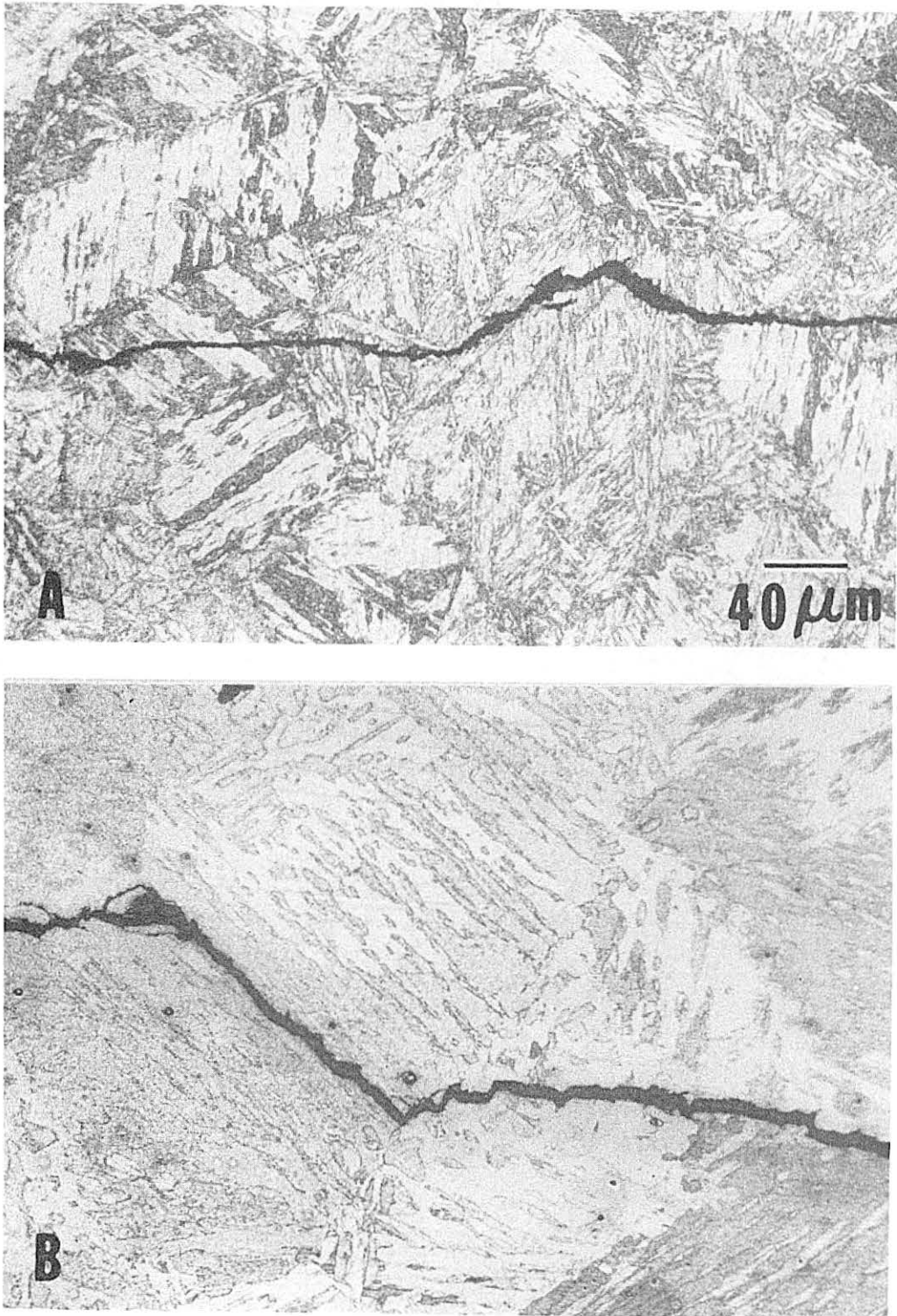
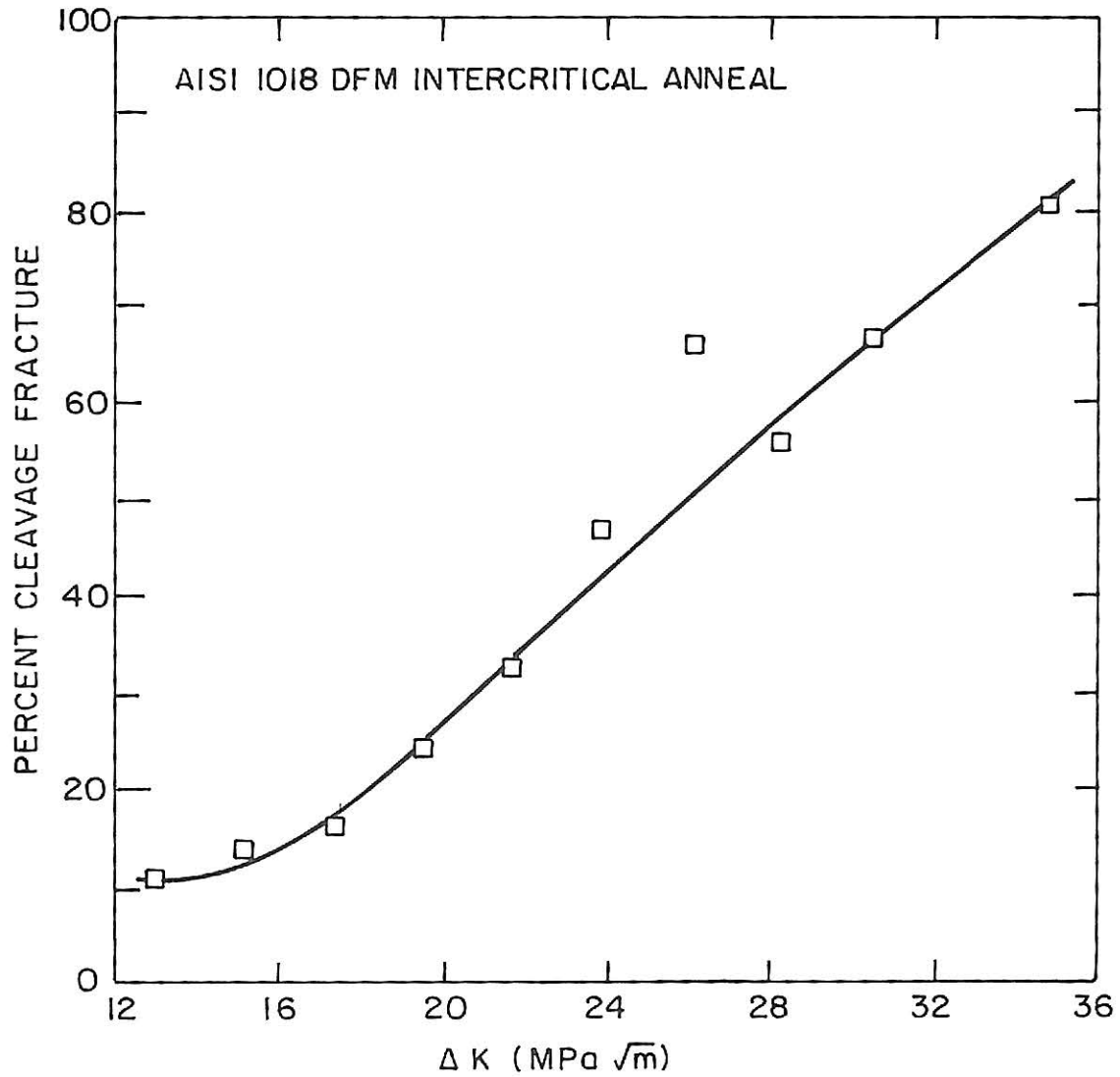


Fig. (15)

XBB 825-4286



XBL822-5152

Fig. (16)



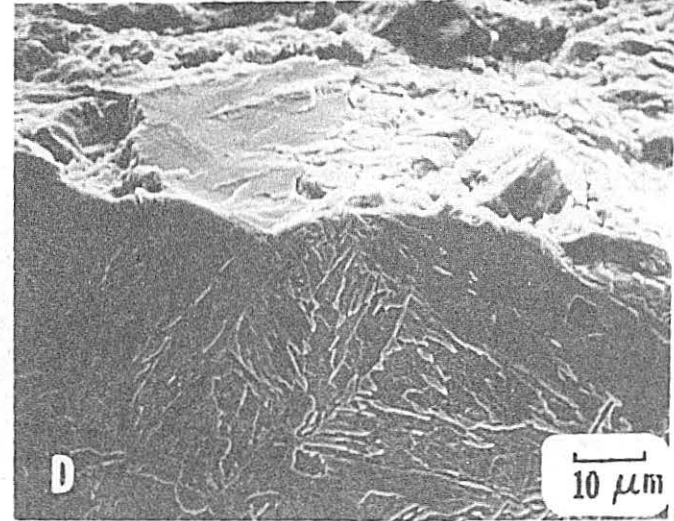
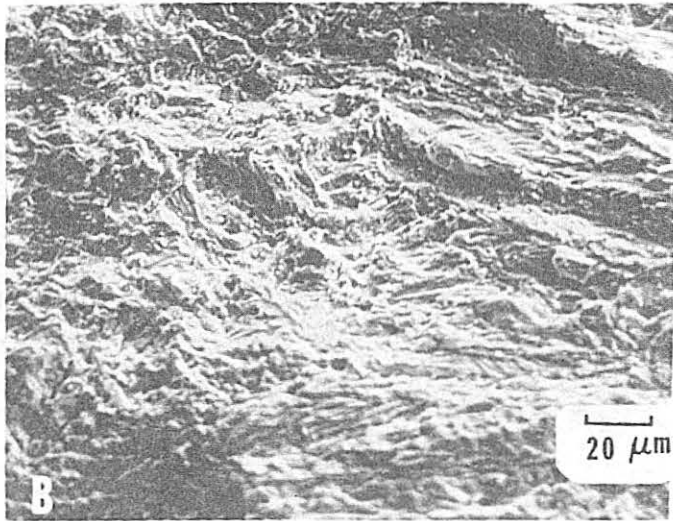
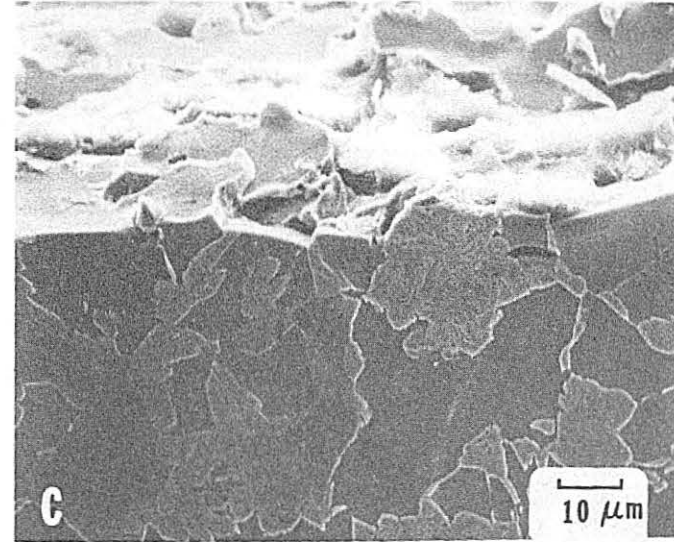
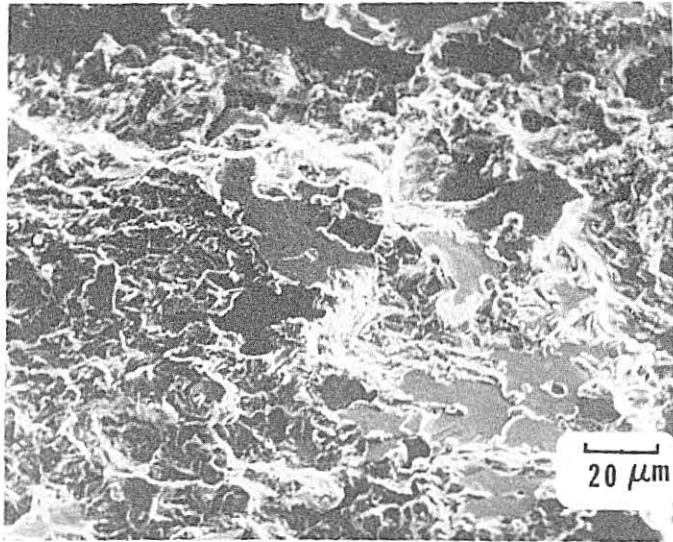


Fig. (17)

XBB 821-805



XBB 825-4284

Fig. (18)

This report was done with support from the Department of Energy. Any conclusions or opinions expressed in this report represent solely those of the author(s) and not necessarily those of The Regents of the University of California, the Lawrence Berkeley Laboratory or the Department of Energy.

Reference to a company or product name does not imply approval or recommendation of the product by the University of California or the U.S. Department of Energy to the exclusion of others that may be suitable.



TECHNICAL INFORMATION DEPARTMENT  
LAWRENCE BERKELEY LABORATORY  
UNIVERSITY OF CALIFORNIA  
BERKELEY, CALIFORNIA 94720